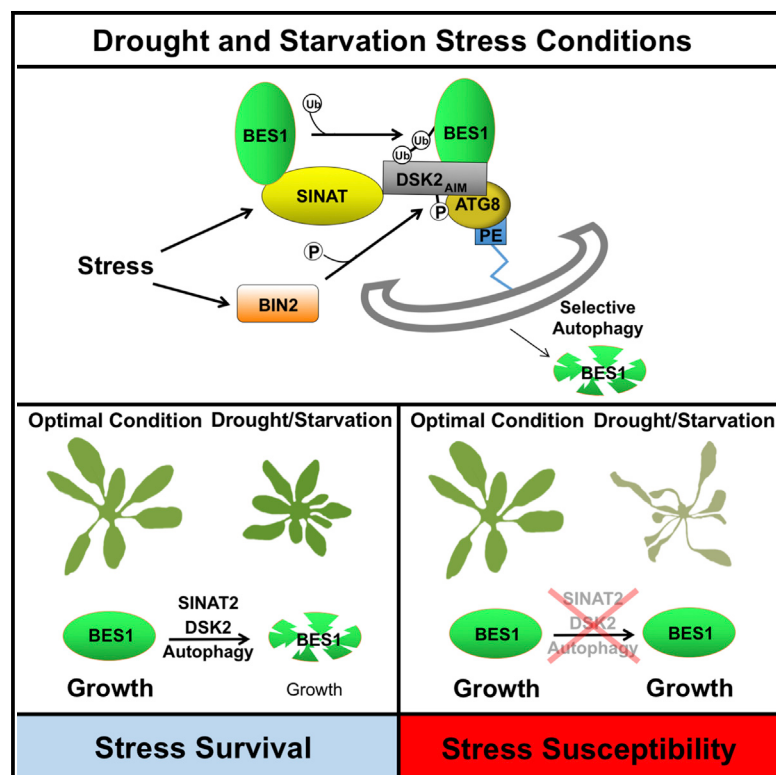


Developmental Cell

Selective Autophagy of BES1 Mediated by DSK2 Balances Plant Growth and Survival

Graphical Abstract



Authors

Trevor M. Nolan, Benjamin Brennan,
Mengran Yang, ..., Diane C. Bassham,
Justin Walley, Yanhai Yin

Correspondence

yin@iastate.edu

In Brief

Plants must carefully balance growth and survival. Nolan et al. show that brassinosteroid-regulated and growth-promoting transcription factor BES1 is degraded during drought and starvation stress via DSK2, a phosphorylation-regulated selective autophagy receptor, thus revealing a mechanism that allows plants to shut down growth during unfavorable conditions.

Highlights

- BES1 is targeted to selective autophagy by ubiquitin receptor DSK2
- BIN2 phosphorylates DSK2, enhancing DSK2's interaction with ATG8
- BES1 is ubiquitinated by SINAT2 during starvation stress
- Impaired BES1 degradation results in compromised drought and starvation survival

Selective Autophagy of BES1 Mediated by DSK2 Balances Plant Growth and Survival

Trevor M. Nolan,¹ Benjamin Brennan,¹ Mengran Yang,² Jiani Chen,¹ Mingcai Zhang,³ Zhaohu Li,³ Xuelu Wang,² Diane C. Bassham,¹ Justin Walley,⁴ and Yanhai Yin^{1,5,*}

¹Department of Genetics, Development and Cell Biology, Iowa State University, Ames, IA 50011, USA

²College of Life Science and Technology, Huazhong Agricultural University, Wuhan 430070, China

³Department of Agronomy, China Agricultural University, Beijing 100193, China

⁴Department of Plant Pathology and Microbiology, Iowa State University, Ames, IA 50011, USA

⁵Lead Contact

*Correspondence: yin@iastate.edu

<http://dx.doi.org/10.1016/j.devcel.2017.03.013>

SUMMARY

Plants encounter a variety of stresses and must fine-tune their growth and stress-response programs to best suit their environment. BES1 functions as a master regulator in the brassinosteroid (BR) pathway that promotes plant growth. Here, we show that BES1 interacts with the ubiquitin receptor protein DSK2 and is targeted to the autophagy pathway during stress via the interaction of DSK2 with ATG8, a ubiquitin-like protein directing autophagosome formation and cargo recruitment. Additionally, DSK2 is phosphorylated by the GSK3-like kinase BIN2, a negative regulator in the BR pathway. BIN2 phosphorylation of DSK2 flanking its ATG8 interacting motifs (AIMs) promotes DSK2-ATG8 interaction, thereby targeting BES1 for degradation. Accordingly, loss-of-function *dsk2* mutants accumulate BES1, have altered global gene expression profiles, and have compromised stress responses. Our results thus reveal that plants coordinate growth and stress responses by integrating BR and autophagy pathways and identify the molecular basis of this crosstalk.

INTRODUCTION

Organisms encounter constantly changing environments and must respond appropriately to optimize their fitness and ensure survival. Growth and stress response programs generally antagonize one another, and as such need to be balanced (Claeys and Inze, 2013; Lopez-Maury et al., 2008). This need is exacerbated in sessile organisms such as plants that cannot easily relocate to escape adverse environmental conditions. Plants are therefore an excellent system for the study of coordination of growth and stress responses, and research in this area has important implications in optimizing plant growth under adverse environments (Skirycz et al., 2011).

Brassinosteroids (BRs) are one major family of growth-promoting plant hormones (Li and Chory, 1997). BRs are perceived by a receptor kinase, BRASSINOSTEROID INSENSITIVE 1

(BRI1), and many other signaling components, to regulate the BRI1-EMS SUPPRESSOR 1 (BES1) and BRASSINAZOLE-RESISTANT 1 (BZR1) family of transcription factors (Clouse, 2011). In the absence of BRs, a GSK3-like kinase BIN2 (Li and Nam, 2002) phosphorylates and inhibits BES1/BZR1 function through multiple mechanisms (Li and Jin, 2007). In the presence of BR, BIN2 kinase activity is inhibited, thus leading to the accumulation of dephosphorylated BES1/BZR1 in the nucleus to regulate target gene expression (Belkhadir and Jaillais, 2015; Guo et al., 2013). Recently, BR signaling has also been linked with stress responses, in part through BIN2 activity (Youn and Kim, 2015; Hao et al., 2013), but many molecular details are still unclear.

Post-translational regulation adds another level of complexity to BR signaling. BES1 and BZR1 can be degraded by the proteasome (Wang et al., 2013; He et al., 2002), and gain-of-function *bes1-D* or *bzr1-D* mutants exhibit stabilized BES1 or BZR1, respectively (Wang et al., 2002; Yin et al., 2002). BES1 is targeted for ubiquitin-mediated degradation by the Skp-CULLIN-F-box (SCF) E3 ubiquitin ligase MORE AXILLARY GROWTH LOCUS 2 (MAX2) during strigolactone-mediated control of shoot branching (Wang et al., 2013), and BZR1 is degraded in a COP1-dependent manner in response to darkness (Kim et al., 2014). These results demonstrated that regulated proteolysis of BES1/BZR1 plays important roles in diverse plant responses, and the key downstream components required for such processes remain to be fully defined.

Typically, ubiquitin-mediated protein degradation occurs through proteasome or autophagy pathways (Floyd et al., 2012; Kraft et al., 2010). Autophagy functions in the degradation and recycling of macromolecules and cytoplasmic organelles, often in response to stress conditions (Yang and Bassham, 2015). There is also recent evidence for selective autophagy in plants, whereby specific proteins or organelles are recognized by receptor proteins and degraded, although many details remain to be elucidated (Michaeli et al., 2016). A subset of these receptors contain a ubiquitin-binding domain and an ATG8-interacting motif (AIM), allowing them to recruit ubiquitinated cargo to ATG8-labeled autophagosomes (Floyd et al., 2012). Two such receptors in *Arabidopsis* are the NEXT TO BRCA1 GENE 1 (NBR1) homolog, which mediates degradation of ubiquitinated protein aggregates (Zhou et al., 2013; Svennning et al., 2011), and REGULATORY PARTICLE NON-ATPASE 10 (RPN10), which can target ubiquitinated proteasomes for autophagic degradation (Marshall et al., 2015).

DOMINANT SUPPRESSOR OF KAR 2 (DSK2) is a ubiquitin-binding receptor protein with known connections to protein degradation pathways in yeast, animals, and plants (Lee and Brown, 2012; Lin et al., 2011; Funakoshi et al., 2002). In *Arabidopsis*, two DSK2 paralogs exist as a result of tandem duplication (DSK2A and DSK2B), with 87% amino acid identity (Farmer et al., 2010). Both DSK2 proteins contain an N-terminal ubiquitin-like (UBL) domain that mediates their interaction with the proteasome and a C-terminal ubiquitin-associated (UBA) domain that can bind both K48 and K63 polyubiquitin chains (Lin et al., 2011). Interestingly, studies of the human DSK2 homologs (Ubiquilins) revealed that they can function in autophagy as LC3-interacting partners (Lee et al., 2013).

In this study, we found links between the regulation and activity of DSK2 to BR signaling, which leads to altered plant growth under drought and fixed-carbon starvation conditions. Specifically, we show that BES1 is targeted for autophagy-mediated degradation by direct interaction with DSK2 following abiotic stress. In addition, the interaction between DSK2 and ATG8 is regulated by BIN2 phosphorylation of DSK2. Loss-of-function *dsk2* mutants have increased BES1 protein levels, altered global gene expression profiles, and compromised survival during stresses. Our results thus provide a previously unknown mechanism by which plants coordinate growth and stress responses by targeting a central growth regulator to the selective autophagy pathway via a phosphoregulated receptor protein.

RESULTS

BES1 Is Degraded through Autophagy and Proteasome Pathways

Although BES1 is known to be degraded in a ubiquitin-dependent manner, the role of autophagy in this process has not been extensively examined. To test the possibility that BES1 is regulated by autophagy in addition to the proteasome, we first investigated BES1 protein levels after treatment with concanamycin A (ConA), the cysteine protease inhibitor E64d, or MG132. ConA and E64d cause accumulation of proteins degraded by autophagy whereas MG132 blocks proteasomal degradation (Kisselev et al., 2012; Inoue et al., 2006; Droege et al., 1993). Remarkably, BES1 accumulated in response to inhibitors of both pathways (Figure 1A) while another transcription factor, RD26, accumulated after MG132 treatment, but not following treatment with ConA or E64d (Figure S1A). This indicates that BES1 can be degraded by both the autophagy and proteasome pathways, similar to HIF2 α in hypoxia response (Liu et al., 2014) and β -catenin in the Wnt signaling pathway (Petherick et al., 2013). To further verify that BES1 is degraded via autophagy, we examined BES1 accumulation in the autophagy-deficient mutants *atg5-1* and *atg7-2* (Chung et al., 2010). Consistently, we found that BES1 protein levels accumulated in these autophagy-deficient mutants during mock treatments and that the application of autophagy inhibitors had no effect in these mutant backgrounds (Figure 1B). Quantification of BES1 protein levels showed that *atg5-1* and *atg7-2* plants had higher BES1 levels after treatment with MG132 compared with mock-treated controls (Figure S1B). Further, coapplication of MG132 with ConA in wild-type (WT) plants led to slightly increased levels of BES1 compared with the application of either

inhibitor alone (Figure S1C, lanes 2, 3, and 5). These results indicate that BES1 can be degraded by both proteasome and autophagy pathways, but that the two pathways do not function completely redundantly, which is consistent with previous reports regarding proteins targeted by both proteasome- and autophagy-mediated degradation (Liu et al., 2014).

Since ubiquitination often triggers degradation through the proteasome and autophagy pathways, we analyzed BES1 ubiquitination. Immunoprecipitated BES1-GFP showed extensive high molecular weight laddering after MG132 or E64d treatment, reminiscent of ubiquitination (Figure 1C). These high molecular weight forms of BES1 cross-reacted with anti-ubiquitin antibody, indicating that ubiquitinated BES1 accumulates in response to proteasome and autophagy inhibitors. Furthermore, treatments of protoplasts expressing BES1-YFP with ConA resulted in accumulation of BES1-YFP in puncta within the vacuole, consistent with BES1 degradation through autophagy (Figure 1D). Similar results were obtained using BES1P:BES1-GFP transgenic lines in which BES1 expression was driven by its native promoter (Figures 1E and 1F), supporting the idea that BES1 puncta observed in protoplasts were not the result of artificially high levels of BES1 expression. Taken together, these results demonstrate that BES1 can be degraded by autophagy.

BES1 Interacts with the Ubiquitin Receptor Protein DSK2

To further explore the mechanisms of BES1 degradation, we performed yeast-two-hybrid screening and identified one of the BES1 interactors as DSK2A, a ubiquitin-binding receptor. We hypothesized that DSK2 might be involved in targeting BES1 for degradation. We first confirmed that BES1 interacts with both DSK2A and DSK2B in vitro using glutathione S-transferase (GST) pull-down and pairwise yeast-two-hybrid assays (Figures 1G and S1D) and also in planta with bimolecular fluorescence complementation (BiFC) and coimmunoprecipitation (coIP) (Figures 1H, S1E, and S1F). Coexpression of BES1-YFPN with DSK2A-YFP-C resulted in strong YFP fluorescence signals (Figure 1H, left panels), some of which were present in mobile puncta (Figure 1I). Fluorescence signals were not observed in negative controls (Figure 1H, middle panels and Figure S1E, lower panels) and were greatly diminished when the ubiquitin-binding UBA domain of DSK2 was deleted (DSK2 Δ UBA) (Figure 1H, right panels), indicating that efficient binding of BES1 to DSK2 in vivo may be promoted by ubiquitination of BES1. Consistent with this idea, coIP using DSK2A-GFP transgenic lines treated with the autophagy inhibitor ConA demonstrated that DSK2A-GFP immunoprecipitated with anti-GFP antibodies pulled down high molecular weight forms of BES1 (Figure S1F) that likely represent ubiquitinated BES1. We also tested the effect of BES1 phosphorylation on the BES1-DSK2 interaction using BES1 phosphorylated in vitro with BIN2 kinase. DSK2 interacted with both phosphorylated and unphosphorylated BES1, indicating that phosphorylation does not markedly influence the interaction between DSK2 and BES1 in vitro (Figure S1G).

To examine whether BES1-DSK2 BiFC puncta were of autophagic origin, we performed colocalization experiments using the autophagosome marker Cerulean-ATG8e (Liu et al., 2012). Reconstituted YFP signal resulting from coexpression of

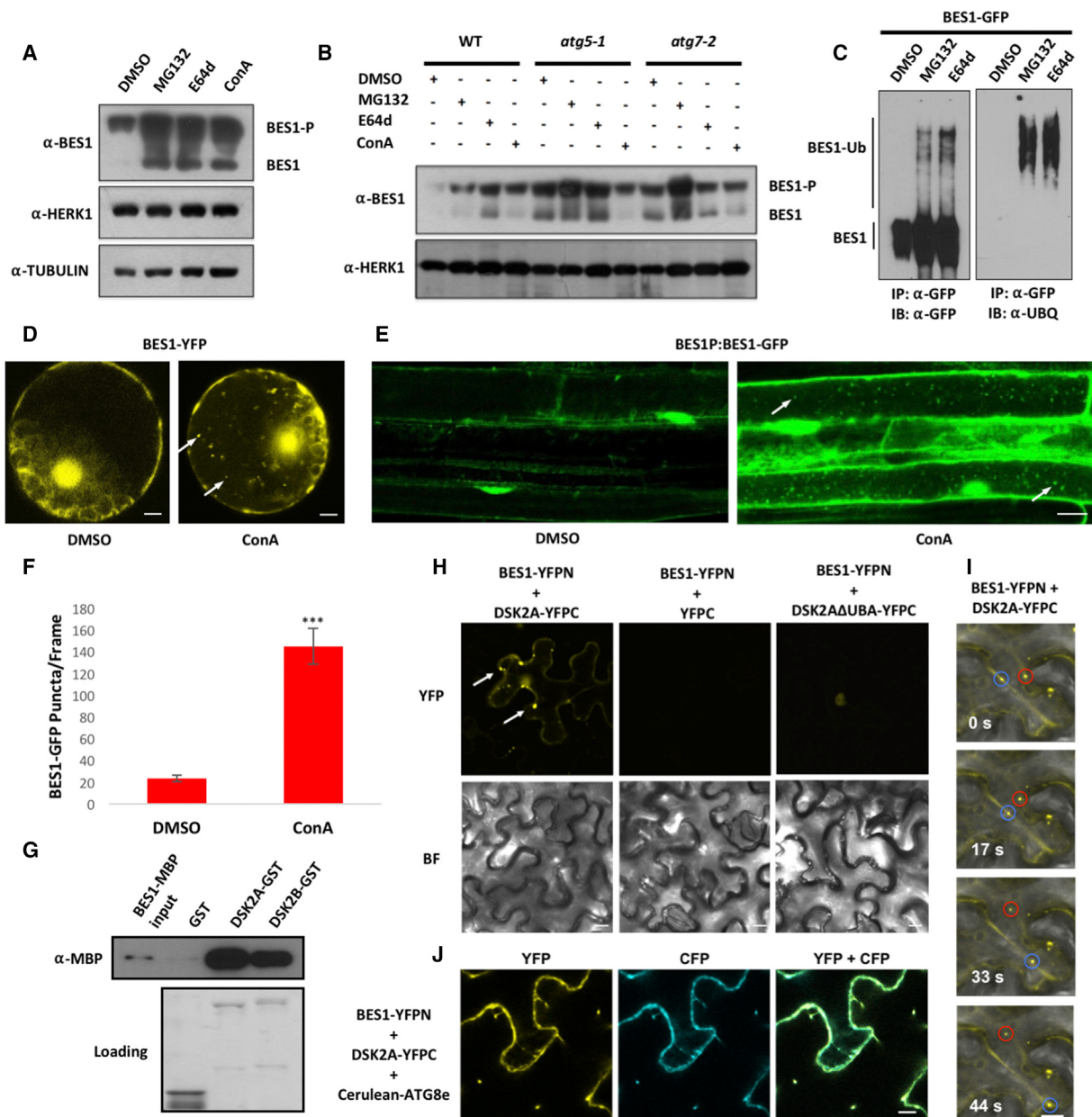


Figure 1. BES1 Is Degraded by Proteasome and Autophagy Pathways and Interacts with Ubiquitin Receptor Protein DSK2

- (A) Response of 10-day-old WT seedlings to proteasome and autophagy inhibitors. Seedlings treated for 6 hr in half-strength Murashige and Skoog medium with DMSO, 50 μM MG132, 20 μM E64d, or 1 μM ConA were analyzed by western blotting with anti-BES1 antibodies. HERK1 and TUBULIN served as loading controls.
- (B) Response of BES1 to inhibitors as described above in 4-week-old WT, *atg5-1*, or *atg7-2* leaf tissue.
- (C) Ubiquitination of BES1. BES1-GFP was expressed in *N. benthamiana* and treated with mock solvent or inhibitors for 16 hr. Immunoprecipitated BES1-GFP was analyzed by western blotting with GFP or ubiquitin antibodies.
- (D) Confocal microscopy images of *Arabidopsis* protoplasts expressing BES1-YFP under –sucrose conditions treated with DMSO or 1 μM ConA for 12 hr. Arrows indicate BES1-YFP puncta. Scale bar represents 5 μm.
- (E) Confocal microscopy of BES1P:BES1-GFP transgenic plants grown for 5 days in light followed by 2 days of sucrose starvation. DMSO or 1 μM ConA was applied 16 hr prior to microscopy. Arrows indicate BES1-GFP puncta. Scale bar represents 20 μm.
- (F) Quantification of BES1P:BES1-GFP puncta. Data represent mean ± SEM, n = 8; ***p < 0.001 (t test).
- (G) GST pull-down showing interactions of GST-DSK2A and GST-DSK2B with BES1-MBP. BES1-MBP was detected using anti-MBP antibody. Loading indicates amounts of GST proteins used in the pull-down reactions.
- (H) Interaction of BES1 with DSK2 in BiFC assays in *N. benthamiana*. Bright-field (BF) images are shown. Arrows indicate BES1-DSK2 puncta.
- (I) Time course showing movement of BES1-DSK2 BiFC signals. Time of image acquisition is shown in seconds.
- (J) Colocalization of BES1-DSK2 BiFC signals (YFP channel) with Cerulean-ATG8e (CFP channel).
- Scale bar for all BiFC experiments represents 10 μm. See also Figure S1.

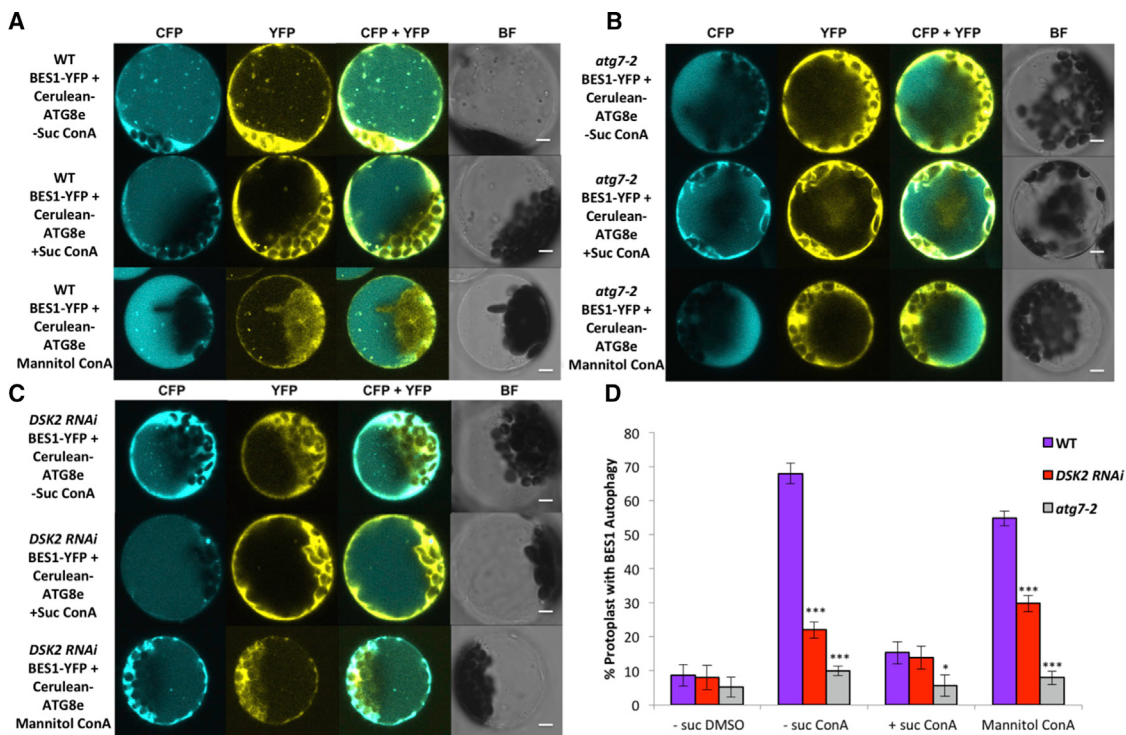


Figure 2. DSK2 Recruits BES1 to ATG8-Labeled Autophagosomes during Stress

(A) Representative images showing colocalization of BES1-YFP and Cerulean-ATG8 in WT *Arabidopsis* protoplasts. Protoplasts treated with control (+Suc), starvation (-Suc), or mannitol stress conditions were incubated with 1 μM ConA for 12 hr and imaged by confocal microscopy. CFP, YFP, or merged (CFP + YFP) fluorescence channels are shown along with bright-field (BF) images.

(B) Colocalization of BES1-YFP and Cerulean-ATG8 in *atg7-2* protoplasts.

(C) Colocalization of BES1-YFP and Cerulean-ATG8 in *DSK2 RNAi* protoplasts.

(D) Quantification of protoplasts with BES1 autophagy. Protoplasts expressing BES1-YFP were treated with indicated treatments as described in (A). BES1 autophagy was defined by the presence of ≥3 autophagosomes per protoplast. Data represent mean of three biological replicates ± SEM, n ≥ 50. *p < 0.05 and **p < 0.001, t test.

Scale bars indicate 10 μm. See also Figure S2.

BES1-YFP with DSK2A-YFPC colocalized extensively with the Cerulean-ATG8e (Figure 1J). DSK2 could also interact with itself (Figures S1E and S1H), in common with several autophagy receptors that often dimerize or multimerize to recruit their cargo for autophagic degradation (Ciuffa et al., 2015; Floyd et al., 2012). YFP signals resulting from interaction of DSK2A-YFP with DSK2A-YFPC also colocalized with Cerulean-ATG8e whereas controls expressing DSK2A-YFP with DSK2A-YFPC or Cerulean-ATG8e alone did not result in any colocalization signal (Figure S1H). DSK2 therefore interacts with BES1 and the DSK2-BES1 complex can localize to autophagosomes, suggesting that DSK2 recruits BES1 to the autophagy pathway.

DSK2 Acts as a Receptor for BES1 Degradation

To test the possibility that DSK2 functions as an autophagy receptor mediating BES1 degradation, we examined colocalization of BES1-YFP with Cerulean-ATG8e in *Arabidopsis* protoplasts under starvation and osmotic stress conditions in which autophagy is induced (Liu et al., 2009; Doelling et al., 2002; Hanaoka et al., 2002). Strong colocalization of BES1-YFP and Cerulean-ATG8e in autophagic bodies occurred upon sucrose starvation (Figure 2A, top panels) or osmotic stress with mannitol treatment (Figure 2A, bottom panels), but not in unstressed con-

trols (Figure 2A, middle panels). The colocalization was not observed in single transformations of BES1-YFP or Cerulean-ATG8e (Figure S2A), indicating that colocalization signals were not an artifact of crosstalk between YFP and CFP channels. Both BES1-YFP and Cerulean-ATG8e puncta were absent in autophagy-deficient *atg7-2* mutants (Figure 2B). On the other hand, *DSK2 RNAi* protoplasts in which both DSK2A and DSK2B were knocked down (Figure S2B) displayed normal ATG8e puncta, but failed to recruit BES1 to ATG8-labeled autophagosomes (Figure 2C), suggesting that DSK2 is required to target BES1 to autophagy but is not required for proper function of the core autophagy machinery. These observations were supported by quantification of protoplasts with visible BES1 autophagy, which was reduced in *DSK2 RNAi* as compared with WT under starvation (-suc) or osmotic (mannitol) stress (Figures 2D and S2C). In contrast, quantification of protoplasts displaying ATG8e autophagy did not reveal significant differences between WT and *DSK2 RNAi* (Figure S2D); confirming that bulk autophagy is not impaired in *DSK2 RNAi*. Furthermore, accumulation of BES1 was observed in *DSK2 RNAi* lines during mock inhibitor treatments, and *DSK2 RNAi* had reduced response to application of E64d or MG132 (Figure 3A), consistent with a role for DSK2 in degrading BES1.

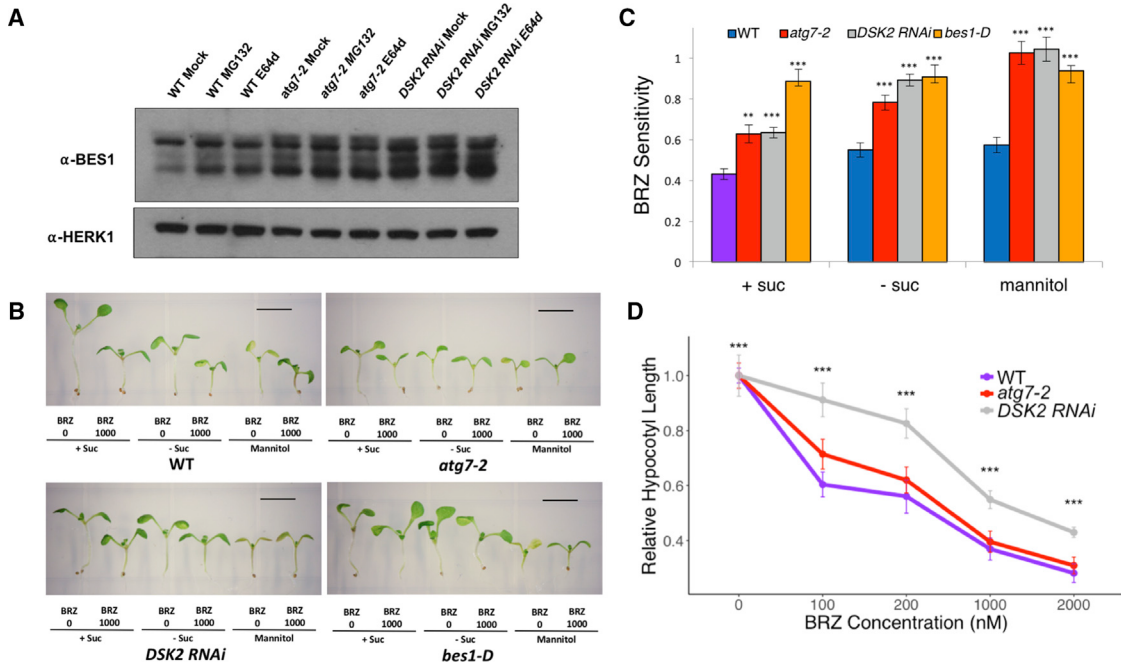


Figure 3. BES1 Degradation by DSK2 and Autophagy Affects BR-Regulated Plant Growth Responses

(A) BES1 accumulation in 4-week-old *Arabidopsis* plants following 6-hr inhibitor treatments. HERK1 was used as a loading control.
(B) BRZ treatments under stress conditions. Five-day-old plants were transferred to medium with indicated combinations of BRZ with or without sucrose or 350 mM mannitol to induce stress. Plants were incubated in darkness for 3 days followed by imaging and hypocotyl measurements. Scale bars represent 5 mm.
(C) Quantification of BRZ sensitivity (hypocotyl length BRZ 1,000 nM/hypocotyl length BRZ 0) from (B). **p < 0.01 and ***p < 0.001, t test.
(D) Response to BRZ under non-stress conditions. Data represent mean ± SEM. ***p < 0.001, t test.

See also Figure S3.

To investigate the effects of stress-induced BES1 degradation on BR-mediated plant growth responses, we measured hypocotyl lengths of WT, *DSK2 RNAi*, *atg7-2*, and *bes1-D* treated with sucrose starvation or mannitol-induced osmotic stress. Under stress conditions, *DSK2 RNAi* and *atg7-2* displayed decreased sensitivity to the BR biosynthesis inhibitor brassinazole (BRZ) (Asami et al., 2000) (Figures 3B and 3C). *DSK2 RNAi* seedlings showed a mild BRZ-resistant phenotype under normal conditions, whereas *atg7-2* was not significantly different than WT, and *bes1-D* was resistant to BRZ under all of the tested conditions (Figures 3D, S3A, and S3B). The BR response phenotype was consistent across two *DSK2 RNAi* lines (Figure S3C) that have been previously well characterized (Lin et al., 2011) and showed depleted DSK2 levels as monitored by immunodetection with anti-DSK2 antibodies (Figure S1D). These results indicate that DSK2 functions as an autophagy receptor during stress conditions to reduce BR-mediated plant growth and imply that DSK2 may also operate in an autophagy-independent manner in non-stress conditions, which is consistent with the known role of DSK2 in other protein degradation pathways (Farmer et al., 2010).

DSK2 Is Phosphorylated by BIN2 and Serves as a Phosphoregulated Autophagy Receptor

Since autophagy receptor proteins typically interact with ATG8, we tested the interaction of DSK2 with several representative ATG8 family members (Marshall et al., 2015; Yoshimoto et al.,

2004). DSK2 physically interacted with all ATG8 members tested in GST pull-down assays, including ATG8e (Figure 4A). To further characterize the role of DSK2 as a possible autophagy receptor, we examined the DSK2 protein sequence for predicted ALMs using iLIR prediction software (Kalvari et al., 2014). ALMs are typified by the consensus sequence W/F/Y-X-X-L/I/V, which is often adjacent to acidic or phosphorylated residues (Kalvari et al., 2014). DSK2A has two regions with high-scoring ALMs, each of which is surrounded by multiple BIN2 consensus phosphorylation sites (S/T-X-X-S/T) (Figure 4B) (Zhao et al., 2002). This observation led us to hypothesize that DSK2 might be phosphorylated proximal to its ALM sequences by BIN2, thereby promoting physical interaction between DSK2 and ATG8 (Farre et al., 2013; Zhu et al., 2013; Wild et al., 2011). Further examination of the DSK2A (hereafter referred to as DSK2) protein sequence revealed 22 potential BIN2 phosphorylation sites (Figure 4B). We first performed phosphatase treatments of immunoprecipitated DSK2-GFP protein, which caused DSK2 to shift from a higher- to lower-migrating form. Thus, DSK2 can be phosphorylated in vivo (Figure 4C).

Next, we found that DSK2 interacts with and is phosphorylated by BIN2, consistent with the predicted BIN2 phosphorylation sites. Specifically, we observed physical association between DSK2 and BIN2 in BiFC assays (Figure 4D), yeast-two-hybrid assays (Figure S4A), and in vitro pull-down assays (Figure S4B). BIN2 efficiently phosphorylated DSK2 in in vitro kinase assays (Figure 4E). Phosphorylation was unaffected by

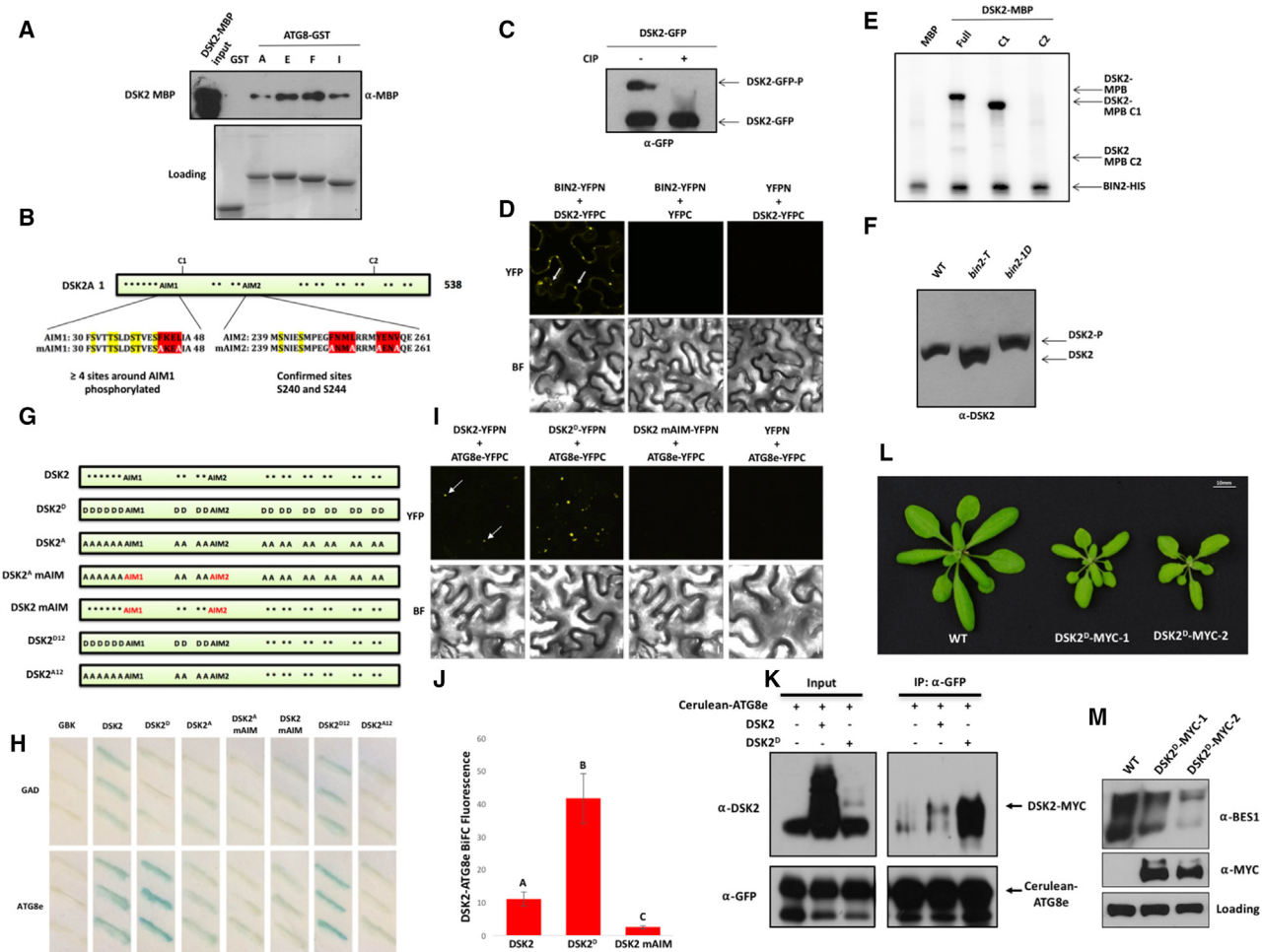


Figure 4. DSK2 Interacts with ATG8 and Is Phosphorylated by BIN2 Kinase around AIMs

(A) Interaction of DSK2 with ATG8 family members in GST pull-down assays. DSK2A-MBP was detected with anti-MBP antibodies. Loading indicates amounts of GST proteins used in pull-down reactions.

(B) Schematic showing DSK2A protein sequence. Text colors indicate the following: red, predicted ATG8 interacting motifs (AIMs); white, AIM mutations present in DSK2 mAIM constructs; yellow, putative BIN2 phosphorylation sites (also marked with an asterisk in the schematic).

(C) Phosphatase treatment of DSK2-GFP expressed in *N. benthamiana*, immunoprecipitated with anti-GFP antibodies and treated with (+) or without (-) calf intestinal alkaline phosphatase (CIP) followed by Phos-tag SDS-PAGE and western blotting with anti-GFP antibodies.

(D) Interaction of BIN2 (BIN2-YFPN) with DSK2 (DSK2-YFPC) in *N. benthamiana* BiFC experiments. Arrows indicate signal from DSK2-BIN2 interaction.

(E) In vitro phosphorylation of DSK2 by BIN2. MBP or DSK2-MBP proteins (Full, aa 1–538; C1, aa 90–538; C2, aa 403–538) were phosphorylated by BIN2 kinase. Arrows indicate phosphorylated DSK2A or BIN2 autophosphorylation.

(F) Modulation of DSK2 phosphorylation by BIN2 in vivo as monitored by Phos-tag SDS-PAGE and western blotting with anti-DSK2 antibody. Arrows denote gel shifts indicating phosphorylated or unphosphorylated DSK2.

(G) Schematics of DSK2 proteins showing mutated BIN2 phosphorylation sites and AIM mutations. Predicted BIN2 phosphorylation sites are marked with an asterisk. When mutated, residues are represented as A (Ser or Thr to Ala) or D (Ser or Thr to Asp). AIM domains are indicated, with red color representing mutant AIMs (mAIM).

(H) Yeast two-hybrid interaction of DSK2 with ATG8e as detected by β -galactosidase (LacZ) activity.

(I) BiFC assays of DSK2 (DSK2-YFPN), phosphomimic forms of DSK2 (DSK2^D-YFPN), or DSK2 AIM mutant (DSK2^{mAIM}-YFPN) with ATG8e (ATG8e-YFPC) in *N. benthamiana*. Arrows indicate signal from DSK2-ATG8 interactions.

(J) Quantification of DSK2-ATG8e BiFC signal from (I). Fluorescence was measured using ImageJ and normalized to controls expressing DSK2-YFPN with YFPC or ATG8e-YFPC with YFPN. Data represent mean of four independent images \pm SEM. Different letters indicate statistically significant differences at $p < 0.05$ (t test).

(K) Coimmunoprecipitation in *N. benthamiana* showing that Cerulean-ATG8e immunoprecipitated with GFP-Trap interacts more strongly with DSK2^D-MYC than DSK2-MYC.

(L) Phenotype of two independent T2 transgenic lines overexpressing phosphomimic DSK2 plants (DSK2^D-MYC).

(M) BES1 protein levels in DSK2^D-MYC lines. Protein extracts from indicated lines were analyzed by western blotting. DSK2^D-MYC was detected with anti-MYC antibodies, while BES1 was detected with anti-BES1. A non-specific band from anti-MYC was used as a loading control.

All DSK2 constructs presented in this figure are derived from the *DSK2A* gene. See also Figure S4.

deletion of the N-terminal UBL domain of DSK2 (DSK2 C1, amino acids [aa] 90–538), but was blocked in a truncated version of DSK2 (DSK2 C2, aa 402–538) that removed 18 of the 22 predicted BIN2 sites (Figures 4B and 4E).

We confirmed that BIN2 phosphorylates DSK2 in vivo by western blotting using anti-DSK2 antibodies coupled with Phos-tag SDS-PAGE, which causes slower migration of phosphorylated proteins (Kinoshita et al., 2006). In this assay, BIN2 loss-of-function *bin2-3 bil1 bil2* triple mutants (*bin2-7*) (Yan et al., 2009) displayed decreased DSK2 phosphorylation (Figure 4F). Conversely, gain-of-function (*bin2-1D*) mutants (Li and Nam, 2002) showed slower migration of DSK2 due to increased phosphorylation (Figure 4F).

To test the effect of BIN2 phosphorylation on DSK2 function, we generated a series of mutants, changing BIN2 sites to aspartic acid (D) or alanine (A) to mimic or abolish phosphorylation, respectively. We found that at least a portion of these sites can be phosphorylated in vivo since coexpression of DSK2-MYC with BIN2 in *Nicotiana benthamiana* led to a higher-migrating form of DSK2, but no shift was observed when BIN2 was expressed with DSK2^A, a construct in which all putative BIN2 phosphorylation sites were mutated to alanine (Figure S4C).

Given the precedence for phosphorylation in increasing autophagy receptor interactions with ATG8 (Wild et al., 2011), we selected ATG8e as a representative ATG8 family member for the investigation of the effect of phosphorylation on interaction of DSK2 with ATG8 (Figures 4G and 4H). Using yeast-two-hybrid assays we found that WT DSK2 interacted with ATG8e, and a phosphomimic version of DSK2 (DSK2^D) had increased interaction with ATG8e (Figure 4H, columns 2 and 3). In contrast, loss-of-function (DSK2^A) mutants showed decreased interaction (Figure 4H, column 4). The phosphomimic mutation of the putative phosphorylation sites proximal to the AIM domains (DSK2^{D12}) was sufficient to increase the interaction of DSK2 with ATG8e (Figure 4H, column 7). Moreover, mutation of the AIM sequences of DSK2 abolished the interaction with ATG8e (Figure 4H, columns 5 and 6). These DSK2 mutants showed a similar trend when tested in plants using BiFC. Specifically, DSK2^D showed increased interaction with ATG8e compared with DSK2 while mutation of DSK2 AIMs in DSK2^{mAIM} also abolished the interaction in planta (Figures 4I and 4J). Furthermore, coIP assays demonstrated that immunoprecipitated Cerulean-ATG8e interacted more strongly with phosphomimic DSK2^D-MYC than with DSK2-MYC (Figure 4K), confirming that phosphorylation of DSK2 promotes interaction with ATG8 in vivo.

We next confirmed site-specific phosphorylation of DSK2 by BIN2 using peptide mass spectrometry. Several phosphorylated peptides were detected from DSK2-MBP phosphorylated in vitro with BIN2-MBP (Tables S1 and S2), whereas no phosphorylation was detected in mock-treated DSK2-MBP. These phosphorylation sites include at least four phosphorylated residues near AIM1 (four sites between aa 5 and 41) and two residues around AIM2 (S240 and S244), suggesting that BIN2 can phosphorylate DSK2 proximal to its AIM domains. To investigate the function of DSK2 phosphorylation on plant growth and BES1 stability, we generated transgenic plants overexpressing phosphomimic DSK2 (DSK2^D). These lines exhibited reduced growth compared with WT plants and had decreased BES1 protein levels (Figures 4L and 4M), consistent with the role of phosphorylated DSK2 in

promoting BES1 degradation. In contrast, transgenic lines expressing inactive DSK2^A or DSK2^{mAIM} variants did not cause dramatic changes in plant growth or BES1 protein levels under the conditions tested (Figures S4D and S4E). Taken together, these results demonstrate that DSK2 is a phosphoregulated ATG8-interacting receptor protein mediating BES1 degradation.

DSK2 Is Involved in BES1 Degradation during Drought Stress

Autophagy is induced by numerous stimuli, including nutrient stress and osmotic or drought stress (Liu et al., 2009). Thus, we hypothesized that autophagic degradation of BES1 may occur under such stress conditions. We confirmed that autophagy-defective *atg7-2* plants were susceptible to drought (Zhou et al., 2013) (Figure 5A). We next tested the role of BR responses in drought. Constitutive activation of BR responses in *bes1-D* led to increased susceptibility to drought, while *brl1-301*, a loss-of-function mutant in the BR pathway, was resistant to drought treatments (Figure 5A). Based on these findings, we examined how BES1 levels may be regulated during drought conditions. To simulate drought conditions in a controlled and reproducible manner, we subjected plants to dehydration treatments, which have been widely used to examine plant drought responses (Sakuma et al., 2006; Urao et al., 1993). Following 4 hr of dehydration, BES1 levels were substantially reduced in WT plants, while BES1 accumulated in *atg7-2* and *DSK2 RNAi* under control conditions and minimal reduction was observed in response to dehydration (Figure 5B). BES1 levels followed a similar trend in plants treated with sublethal drought in soil (Figure 5C), showing accumulation in *DSK2 RNAi* and *atg7-2* backgrounds. Accumulation of BES1 in the mutant backgrounds was not due to increased transcription, as BES1 expression levels were not markedly increased in *DSK2 RNAi* or *atg7-2* compared with WT during control or stress conditions (Figures S5A and S5B). Moreover, experiments in which translation was inhibited via cycloheximide (CHX) treatment showed that BES1 stability was decreased to a greater extent in drought versus control treated WT plants, especially at later time points of CHX treatment (Figures 5D [top panels] and S5C), whereas a similar reduction in BES1 was not observed after drought and CHX treatment in *DSK2 RNAi* or *atg7-2* plants (Figure 5D, middle and bottom panels). These results demonstrate that BES1 is regulated at the post-translational level during drought stress.

Since *DSK2 RNAi* plants have elevated BES1 levels under drought conditions, we expected them to behave similarly to *bes1-D*. In support of this hypothesis, *DSK2 RNAi* plants also had drastically reduced survival in drought assays (Figures 5A, 5E, and S6A), and lost water more quickly in detached leaf water loss assays (Figure 5F). Meanwhile, *DSK2* expression remained decreased in *DSK2 RNAi* compared with WT under stress conditions (Figures S5D and S5E).

Given the strong phenotype of *DSK2 RNAi* under drought conditions, we next examined changes in the transcriptome during control and dehydration conditions using RNA sequencing (RNA-seq). In dehydrated WT plants, 554 genes were differentially expressed (DE) compared with mock-treated controls (dehydration DE genes; Table S3). These dehydration-responsive transcripts exhibit a high concordance with previously published

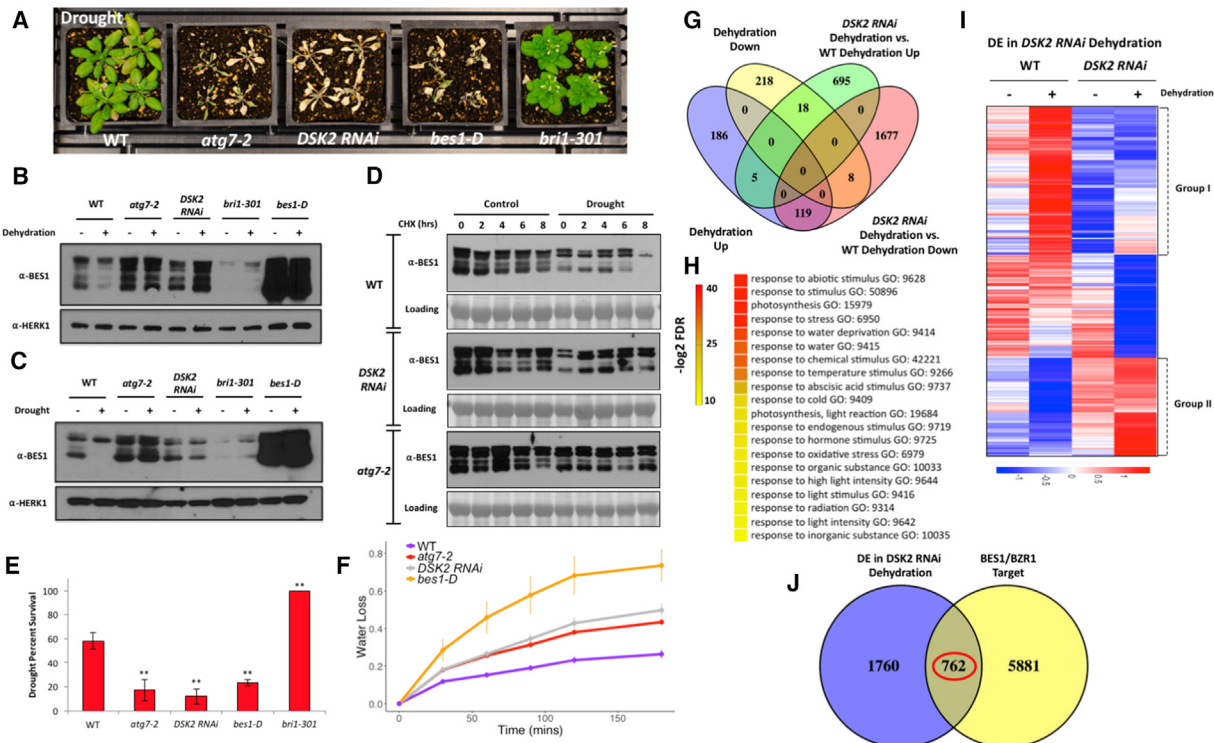


Figure 5. Degradation of BES1 Mediated by DSK2 and Autophagy during Drought Stress

- (A) Plant phenotypes for indicated lines after drought recovery assays.
 - (B) BES1 protein levels during dehydration. Plants were subjected to control or 4-hr dehydration conditions and BES1 levels analyzed by western blotting. HERK1 was used as a loading control.
 - (C) BES1 protein levels during drought in soil. Plants were treated with control (well-watered) or sublethal drought conditions, and protein was extracted from plant leaf tissue for analysis by western blotting as described in (B).
 - (D) BES1 protein levels following cycloheximide (CHX) treatment during control or drought treatments. Indicated genotypes were grown for 4 weeks in control or sublethal drought conditions followed by treatment with 500 µM CHX for the indicated time points. Ponceau S staining was used as loading control.
 - (E) Quantification of percent survival following drought recovery. Plants producing new leaves after the 7-day recovery period were scored as survivors. Data represent mean survival of three biological replicates of 12–16 plants ± SEM. **p < 0.01 (t test).
 - (F) Detached leaf water loss assays. Water loss represents proportion of total weight lost compared with initial weight. Data represent mean ± SEM from two to three biological replicates. Differences between WT and mutants are statistically significant at p < 0.05 for all time points shown except 30 min (t test).
 - (G) Comparison of dehydration-regulated and DSK2 RNAi dehydration DE genes in whole-transcriptome RNA-seq.
 - (H) Top 20 significantly enriched GO terms in DSK2 RNAi dehydration DE genes as ranked by false discovery rate (FDR).
 - (I) Clustering of 2,522 genes differentially expressed in DSK2 RNAi dehydration versus WT dehydration. Color legend indicates normalized gene expression values.
 - (J) Comparison of DSK2 RNAi dehydration DE genes with BES1/BZR1 target genes from genome-wide chromatin immunoprecipitation datasets.
- See also Figures S5–S7.

dehydration datasets and an enrichment of drought-related gene ontology (GO) terms (Figures S6B and S6C). We observed few genes that were DE in *DSK2 RNAi* plants compared with WT under control conditions (Table S3), but strikingly, 2,522 genes were DE in *DSK2 RNAi* compared with WT under dehydration stress (referred to as *DSK2 RNAi* dehydration DE genes). The DE genes in dehydrated *DSK2 RNAi* lines opposed dehydration-regulated genes (Figure 5G) and were enriched for drought- and/or dehydration-related GO terms (Figure 5H). Furthermore, clustering analysis of *DSK2 RNAi* dehydration DE genes (Figures 5I and S6D) revealed many genes with increased expression during dehydration in WT that showed lower expression patterns in *DSK2 RNAi* and minimal induction by the treatment (group I), while others were repressed in WT by dehydration but had higher expression in *DSK2 RNAi* (group II). These transcriptional changes following

dehydration are consistent with the drought-hypersensitive phenotype of the *DSK2 RNAi* mutant.

Many previously published drought-regulated genes (Miyayama et al., 2009) were present in these datasets and showed altered expression in *DSK2 RNAi* lines (Figure S6E). There is also a high degree of overlap between BES1/BZR1 target genes and *DSK2*-regulated genes (Figure 5J and Table S3). Comparison of BR- and dehydration-regulated genes indicated that drought and BR pathways antagonize each other (Figures S6F–S6H). These results demonstrate that perturbation of BES1 levels in *DSK2 RNAi* plants coincides with the dramatic changes in drought phenotypes and drought-related gene expression.

We further confirmed the role of BES1 in drought stress resistance by testing the drought phenotype of previously described *BES1-RNAi* plants (Yin et al., 2005). *BES1 RNAi* had increased

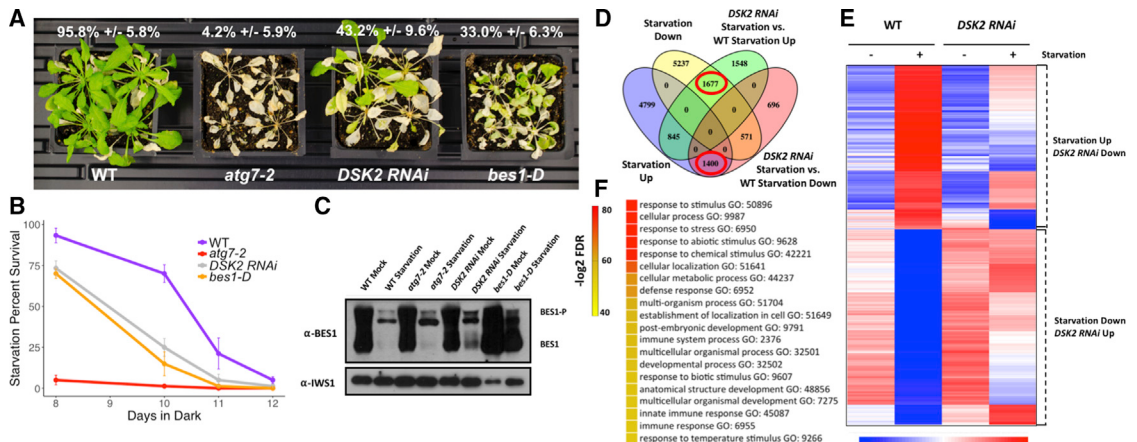


Figure 6. Degradation of BES1 under Fixed-Carbon Starvation via DSK2 and Autophagy

(A) Representative images of plant survival following 8-day fixed-carbon starvation treatment. Percentage survival is indicated from two biological repeats of 7–12 plants \pm SD. Differences between WT and mutants are statistically significant, $p < 0.05$ (t test).

(B) Time course of fixed-carbon starvation survival. Plants were grown on half-strength Linsmaier and Skoog plates without sucrose for 1 week and transferred to darkness for indicated time points followed by 1 week of recovery under light. Data represent mean \pm SEM for three to four biological replicates of 20 plants each. Differences between WT and mutants are statistically significant, $p < 0.05$ (t test).

(C) Western blot analysis of BES1 protein levels following 5-day dark treatment. A general transcription factor, IWS1, served as a loading control.

(D) Comparison of starvation-regulated and *DSK2 RNAi* starvation DE genes in whole-transcriptome RNA-seq.

(E) Clustering analysis of 3,077 genes that are starvation upregulated and downregulated in *DSK2 RNAi* starvation or starvation downregulated and upregulated in *DSK2 RNAi* starvation. Color legend indicates normalized gene expression values.

(F) Top 20 significantly enriched GO terms in *DSK2 RNAi* starvation DE genes as ranked by false discovery rate (FDR).

See also Figure S8.

resistance to drought compared with WT (Figures S7A and S7B) and decreased BES1 protein levels (Figure S7C). We then generated *DSK2 RNAi* *BES1 RNAi* double transgenic plants in which both BES1 and DSK2 were reduced (Figure S7D) to determine the extent to which BES1 accumulation was responsible for the increased drought sensitivity in *DSK2 RNAi*. Drought survival assays indicated that decreased BES1 in *DSK2 RNAi* *BES1 RNAi* plants could restore the drought survival phenotype of *DSK2 RNAi* to near WT levels (Figures S7E and S7F). These observations indicate that BES1 accumulation in *DSK2 RNAi* is a major contributor to the impaired survival of *DSK2 RNAi* plants during drought stress.

We also tested the effect of modulating BIN2 activity on BES1 protein levels and plant survival during drought stress. We found that loss-of-function *bin2-T* mutants had higher BES1 protein levels compared with WT after dehydration treatment, whereas BES1 levels were reduced in gain-of-function *bin2-1D* mutants during dehydration (Figure S7G). Furthermore, *bin2-1D* plants were resistant to drought stress compared with WT. However, *bin2-T* mutants did not show obviously decreased drought survival under the conditions tested (Figures S7H and S7I), likely due to the large array of substrates targeted by BIN2 kinase (Youn and Kim, 2015). Taken together, these results support a role for BIN2 in modulating BES1 protein levels and survival under stress conditions.

DSK2 Is Involved in BES1 Degradation during Fixed-Carbon Starvation

In addition to drought, autophagy is strongly induced under nutrient-limiting conditions, including fixed-carbon starvation,

and autophagy-deficient mutants have reduced survival under carbon or nitrogen starvation (Thompson et al., 2005; Contento et al., 2004). Recently, it has been shown that BRs are required for sugar-promoted hypocotyl elongation in the dark and that BZR1 is both transcriptionally and post-translationally regulated by sucrose, which suggests that BES1/BZR1 protein levels may be controlled under low-energy conditions (Zhang et al., 2015). We confirmed the sensitivity of *atg7-2* to starvation stress in our assays and found that constitutive BR response in *bes1-D* led to enhanced sensitivity to fixed-carbon starvation (Figures 6A and 6B). We next examined BES1 protein levels after 5 days of dark treatment. Fixed-carbon starvation reduced the level of BES1 in WT plants, whereas BES1 was reduced to a lesser extent in *atg7-2* and *DSK2 RNAi* (Figures 6C and S8A). Regulation of BES1 under these conditions was at least partially due to reduced energy availability rather than dark conditions, since addition of sucrose during starvation treatments increased BES1 levels (Figure S8B). Furthermore, we tested the fixed-carbon starvation survival phenotypes of *DSK2 RNAi* lines. In line with the BES1 protein accumulation, *DSK2 RNAi* plants had markedly reduced recovery compared with WT in a fixed-carbon starvation time course with seedlings grown on medium without sucrose (Figures 6B and S8C) or after 8 days of dark treatment on soil-grown plants (Figure 6A). Additionally we tested the role of BIN2 in starvation stress by examining the phenotypes of *bin2* mutants in starvation survival assays. Similar to our observations in drought stress, gain-of-function *bin2-1D* mutants were resistant to starvation; however, *bin2-T* mutants were also more resistant than WT to starvation, raising the possibility that additional BIN2 homologs

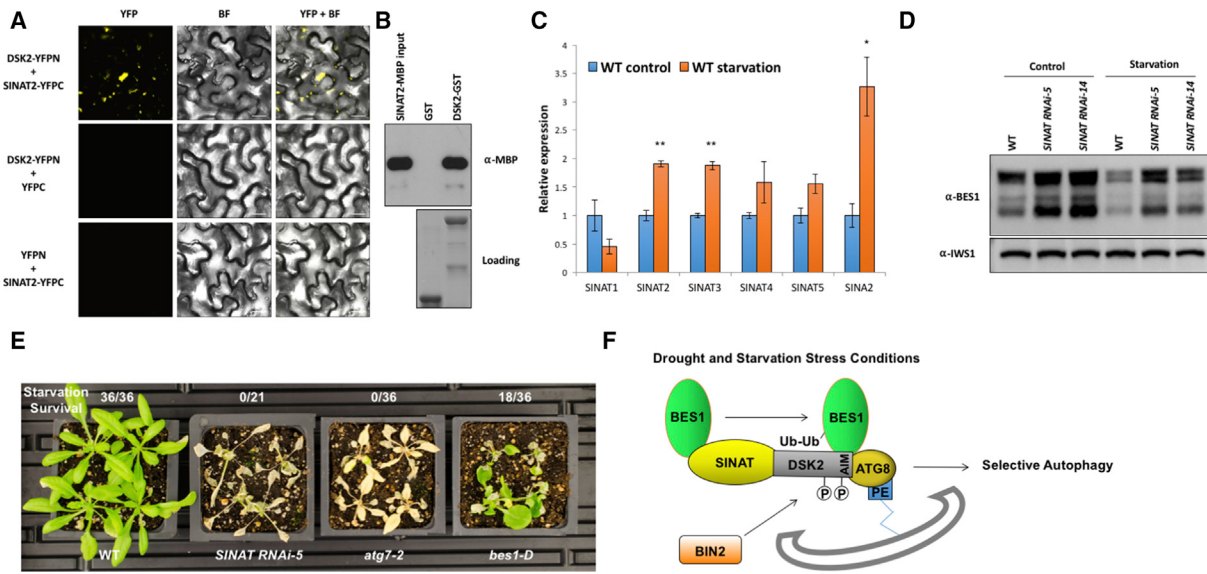


Figure 7. SINAT E3 Ligases Are Involved in BES1 Degradation during Starvation

(A) Interaction of DSK2 and SINAT2 in BiFC assays in *N. benthamiana*. Bright-field (BF) images are shown. Scale bars indicate 10 μ m.
 (B) GST pull-down assays showing interaction of SINAT2 with DSK2. SINAT2-MBP was detected with anti-MBP antibodies. Loading indicates amounts of GST proteins used.
 (C) Expression levels of SINAT family E3 ligases from starvation RNA-seq experiments. Data represent mean \pm SEM. *p < 0.05 and **p < 0.01 (t test).
 (D) Western blot analysis of BES1 protein levels following 3-day starvation treatment. IWS1 served as a loading control.
 (E) Representative images of plant survival following 8 days of fixed-carbon starvation treatment. Numbers indicate recovered plants after a 1-week recovery period. The experiment was repeated twice with similar results.
 (F) A Model for BES1 protein degradation through selective autophagy. Under stress conditions, BES1 is ubiquitinated and targeted for degradation by SINAT E3 ubiquitin ligases, partly due to the induction of *SINAT* genes by stresses. Ubiquitin receptor DSK2 interacts with BES1 and recruits BES1 to autophagy through DSK2-ATG8 interactions. When activated under stress conditions, BIN2 phosphorylates DSK2 flanking DSK2's AIM domains and potentiates DSK2-ATG8 interactions, promoting BES1 degradation through selective autophagy.

See also Figure S9.

or substrates may be regulated during starvation in *bin2-T* mutants (Figure S8D).

We also performed RNA-seq experiments under starvation conditions and found 6,737 genes that were DE in *DSK2 RNAi* lines compared with WT (designated *DSK2 RNAi* starvation DE genes). Examination of these genes showed that starvation-responsive gene expression was attenuated in *DSK2 RNAi* plants as illustrated by the opposing pattern of overlap observed between *DSK2 RNAi* starvation DE genes and genes regulated by starvation in WT. A total of 1,677 out of 4,070 *DSK2 RNAi* starvation upregulated genes and 1,400 of 2,667 *DSK2 RNAi* starvation downregulated genes overlapped with genes downregulated or upregulated in WT starvation, respectively (Figures 6D and S8E). These differential changes were also evident from clustering analysis (Figure 6E). The DE genes in starved *DSK2 RNAi* lines were enriched for GO terms related to plant growth and stress responses (Figure 6F). Further comparisons revealed that many DE genes in starved *DSK2 RNAi* lines are BES1/BZR1 targets (24.7%, 1,664/6,737 genes) (Figure S8F). Moreover, we observed a large degree of overlap among *DSK2 RNAi* starvation DE genes and those DE in *atg7-2* and *bes1-D* during starvation (Figures S8G and S8H), suggesting functional overlap among *DSK2*, *ATG7*, and *BES1*. Furthermore, 41% of BR-induced genes (1,601/3,898) and 33.6% of BR-repressed genes (1,274/3,789) were regulated in opposite directions (down- and upregulated, respectively) during starvation (Figures S8I–S8K), indicating

a mostly inverse relationship between BR function and starvation response. Taken together, these results demonstrate that BES1 and BRs play a negative role in survival during fixed-carbon limitation and that BES1 is degraded by DSK2 and autophagy pathways under these conditions.

SINAT Family E3 Ubiquitin Ligases Are Involved in BES1 Degradation during Starvation

In addition to DSK2, we also recovered a RING E3 ubiquitin ligase, SINAT2, as a BES1-interacting partner via yeast-two-hybrid screening. Several SINAT family members directly interact with and ubiquitinate BES1 (Yang et al., 2017 [this issue of *Developmental Cell*]). To test the possible role of SINAT2 in DSK2-mediated degradation of BES1, we first examined the physical interaction of SINAT2 with DSK2. Strikingly, SINAT2 strongly interacted with DSK2 in BiFC assays (Figure 7A), likely in the nucleus and also in puncta. GST pull-down assays demonstrated that the DSK2-SINAT2 interaction is direct (Figure 7B). These data indicate that SINAT2 and DSK2 form a complex to carry out BES1 degradation and suggest that SINAT family E3 ligases might be involved in targeting BES1 for degradation during stress. SINAT E3 ligases have been previously implicated in stress responses (Bao et al., 2014), and we found that three out of six SINAT family members were transcriptionally induced by starvation (Figure 7C). Furthermore, BES1 protein accumulated following starvation treatment in *SINAT RNAi* lines compared

with WT (Figures 7D and S9A) and *S/NAT RNAi* plants exhibited a starvation hypersensitive phenotype, showing dramatically reduced survival in fixed-carbon starvation assays (Figure 7E). Accordingly, BES1 ubiquitination was reduced in *S/NAT RNAi* plants compared with WT under starvation conditions when autophagy-mediated degradation was blocked with E64d (Figure S9B). These findings reveal that SINAT E3 ubiquitin ligases are involved in targeting BES1 for degradation during starvation (Figure 7F).

DISCUSSION

Organisms develop strategies to coordinate growth and stress responses. Multiple mechanisms have been reported that allow for inhibition of growth when stress is encountered, including global reprogramming of gene expression (Harb et al., 2010), RNA processing or sequestration (Weber et al., 2008), and translation inhibition (Ren et al., 2011). Our studies established a major mechanism for the coordination of plant growth and stress responses. We demonstrated that targeting of a central growth regulator, BES1, to autophagy-mediated degradation by ubiquitin receptor DSK2 plays an important role in slowing down plant growth under dehydration and fixed-carbon starvation (Figure 7F). We showed that GSK kinase BIN2, which is repressed by growth hormone BRs and activated by stresses (Youn and Kim, 2015; Dal Santo et al., 2012; Zhang et al., 2009; Charrier et al., 2002), controls BES1 autophagy by modulating DSK2-ATG8 interaction. Our studies also revealed a function for *S/NATs*, which encode E3 ubiquitin ligases that target the active unphosphorylated form of BES1 to influence BR-regulated growth in a light-dependent manner (Yang et al., 2017 [this issue of *Developmental Cell*]). Our results indicate that *S/NATs* are induced by starvation stress and are involved in targeting BES1 for degradation under starvation conditions. Thus, both BIN2 and SINATs are activated by stress to potentiate BES1 degradation.

Our results revealed crosstalk between autophagy and plant steroid hormone signaling pathways. Both autophagy (Liu et al., 2009; Doelling et al., 2002; Hanaoka et al., 2002) and BRs (Zhang et al., 2015; Hao et al., 2013) have been linked to drought and starvation, but the role of BRs in controlling plant survival and mechanisms regulating BES1 during these stresses is not completely understood. Recently, it was reported that TARGET OF RAPAMYCIN (TOR) functions to activate BR signaling under energy-replete conditions by stabilizing BZR1 and that *tor rna1*-induced BZR1 degradation was attenuated by treatment with 3-methyladenine, an inhibitor of autophagy (Zhang et al., 2016). These results suggest that BZR1 may be degraded through autophagy, but genetic and cell biological evidence for autophagy-mediated degradation of BES1/BZR1 family transcription factors as well as the E3 ligase and autophagy receptor that mediate this process remained to be established. The BES1-DSK2-ATG8 interaction demonstrated in this study provides a molecular mechanism connecting autophagy and BR pathways, which allows plants to slow down growth under stress conditions. Our studies revealed that BES1 negatively regulates plant survival under drought and starvation and that DSK2 mediates degradation of BES1 under these conditions (Figures 5 and 6). Accumulation of BES1 in *DSK2 RNAi* or *atg7-2* mutants coincided with decreased plant survival under

both drought and fixed-carbon starvation. In contrast, *DSK2 RNAi* and *atg7-2* mutants were resistant to the inhibition of BR biosynthesis during stress (Figure 3), suggesting that BES1 accumulation in these mutants promotes plant growth during stress. Furthermore, expression of a constitutive active DSK2 (*DSK2^D*, mimicking BIN2 phosphorylation) led to reduced BES1 protein levels and decreased plant growth (Figure 4). Taken together, these genetic and physiological studies indicate that DSK2-mediated BES1 degradation leads to reduced plant growth under stress conditions and is required for optimal plant responses to stresses.

This study established DSK2 as a selective autophagy receptor. DSK2 has ties to both proteasome and autophagy pathways. The human homologs of DSK2, called Ubiquilins, have been implicated in protein degradation pathways including autophagy as LC3 (ortholog of ATG8) interactors (Lee et al., 2013), but their specific functions in autophagy have not been fully defined. In *Arabidopsis*, DSK2 was shown to participate in ubiquitinated cargo delivery to the proteasome, along with other receptors (Lin et al., 2011; Farmer et al., 2010; Vierstra, 2009). Our results demonstrate that DSK2 targets BES1 through selective autophagy. DSK2 is required for recruitment of BES1 to autophagy, but ATG8-labeled autophagosomes are not affected in *DSK2 RNAi* lines (Figure 2), suggesting that DSK2 functions in selective degradation of BES1 but does not regulate bulk autophagy. Although selective autophagy has been shown to function in plant systems, the full repertoire of autophagy receptors and their specific cargoes is only beginning to be fully appreciated (Michaeli et al., 2016). Multiple lines of evidence demonstrated that BES1-DSK2-ATG8 interactions function to target BES1 to selective autophagy during stress (Figures 1 and 2). Considered together, our results expand the role of DSK2 in ubiquitin-mediated proteolysis by showing DSK2's role in selective autophagy and by providing a molecular basis for DSK2 in targeting specific proteins such as BES1 for degradation.

Another significant finding of this study is that DSK2-ATG8 interaction is modulated by BIN2 kinase, a negative regulator of the BR pathway. BIN2 phosphorylates BES1/BZR1 as well as numerous other substrates involved in diverse aspects of plant growth, development, and stress responses (Youn and Kim, 2015). DSK2 is phosphorylated by BIN2 flanking its AIM domains (Figures 4 and S4), which is a typical pattern of autophagy receptors that are regulated by phosphorylation (Farre et al., 2013; Zhu et al., 2013; Wild et al., 2011). Mutational analysis indicated that DSK2 phosphomimic forms had increased interaction with ATG8, suggesting that BIN2 induces BES1 degradation by phosphorylating DSK2 and enhancing its interaction with the autophagy protein ATG8. These results provide a new layer of regulation of BES1 by BIN2 kinase.

The role of DSK2 in the regulation of BES1 during stress responses is further corroborated by global gene expression studies. Our RNA-seq analyses showed that BES1 accumulation in *DSK2 RNAi* was associated with altered expression of a large number of genes under dehydration and starvation conditions. In contrast, few genes were affected in *DSK2 RNAi* plants in unstressed control conditions, indicating that DSK2 functions primarily during stresses. BES1 and BZR1 bind to the promoters

of about 6,600 target genes as determined by genome-wide chromatin immunoprecipitation studies (Yu et al., 2011; Sun et al., 2010). Strikingly, a large proportion of the misregulated genes under both stress conditions were BES1/BZR1 targets (Figures 5 and S9). These results suggest that BES1 accumulation under stress conditions in *DSK2 RNAi* is associated with changes in BES1/BZR1 target gene expression. Moreover, the expression of stress-regulated genes in dehydration and starvation generally opposed that of BR-regulated genes, indicating that BR responses are reduced during stress through degradation of BES1 by DSK2 and autophagy.

In metazoans, regulation of β-catenin, a positive regulator of cell proliferation in the Wnt pathway, provides a remarkable example of how growth and stress pathways can crosstalk through targeted protein degradation. β-Catenin reduces autophagy and inhibits the expression of the autophagy receptor p62 under normal conditions, but is targeted for degradation through interaction with the autophagy protein LC3 under autophagy-inducing conditions (Petherick et al., 2013). Similarly, our results showed that autophagy-mediated degradation of BES1 under stress conditions affects BR-regulated growth and stress responses; however, whether the BR pathway also influences autophagy remains an open question. Given the similarities in signaling mechanisms between the Wnt and BR signaling pathways (Yin et al., 2002), future studies should determine whether there is a reciprocal regulation of autophagy by BRs, which could provide additional means for plants to balance growth and stress responses.

STAR★METHODS

Detailed methods are provided in the online version of this paper and include the following:

- KEY RESOURCES TABLE
- CONTACT FOR REAGENT AND RESOURCE SHARING
- EXPERIMENTAL MODEL AND SUBJECT DETAILS
 - Plant Materials and Growth Conditions
- METHOD DETAILS
 - Inhibitor Treatments
 - BRZ Response Assays
 - Drought and Dehydration Assays
 - Fixed-Carbon Starvation Assays
 - Immunoprecipitation
 - TUBE Ubiquitination Assays
 - Western Blotting
 - RNA-Seq
 - Yeast-Two Hybrid
 - *In Vitro* Pull-down Assays
 - BiFC Assays
 - Coexpression of DSK2 and BIN2 in Tobacco
 - Plasmid Constructs and Generation of Transgenic Plants
 - Protoplast Transient Expression Assays
 - Confocal Microscopy of *Arabidopsis* Roots
 - Phosphorylation Assays
 - Protein Digestion and LC-MS/MS
- QUANTIFICATION AND STATISTICAL ANALYSIS
 - RNA-seq Data Processing and Statistics
- DATA AND SOFTWARE AVAILABILITY

SUPPLEMENTAL INFORMATION

Supplemental Information includes nine figures and five tables and can be found with this article online at <http://dx.doi.org/10.1016/j.devcel.2017.03.013>.

AUTHOR CONTRIBUTIONS

T.N. performed most of the experiments with the following exceptions: B.B. produced recombinant proteins, performed some of the GST pull-down assays, and assisted in generating DSK2 transgenic lines; M.Y. and X.W. generated SINAT RNAi lines and analyzed BES1 accumulation in SINAT RNAi during starvation; T.N., J.C., M.Z., and Z.L. conducted the RNA-seq experiments; D.C.B. provided autophagy mutants and materials and assisted in analyzing autophagy experiments; J.W. conducted mass spectrometry for identification of DSK2 phosphorylation sites; T.N. and Y.Y. wrote the manuscript with D.C.B. and J.W.

ACKNOWLEDGMENTS

The identification of DSK2 and SINAT2 as BES1 interactors by yeast two-hybrid screens was performed in Dr. J. Chory's laboratory at the Salk Institute for Biological Studies with support from Howard Hughes Medical Institute (HHMI). DSK2 antibodies and *DSK2 RNAi* seeds were a generous gift from Hongyong Fu. We thank Drs. Patrick S. Schnable and Sanzhen Liu (Data2Bio) for assistance in analyzing RNA-seq data and Dior Kelly and Hongqing Guo for critical comments on the manuscript. The work is supported by grants from NIH (1R01GM120316-01A1), NSF (IOS-1257631), and the Plant Science Institute at Iowa State University.

Received: June 17, 2016

Revised: January 17, 2017

Accepted: March 14, 2017

Published: April 10, 2017

REFERENCES

- Asami, T., Min, Y.K., Nagata, N., Yamagishi, K., Takatsuto, S., Fujioka, S., Murofushi, N., Yamaguchi, I., and Yoshida, S. (2000). Characterization of brasinsazole, a triazole-type brassinosteroid biosynthesis inhibitor. *Plant Physiol.* 123, 93–99.
- Bao, Y., Wang, C., Jiang, C., Pan, J., Zhang, G., Liu, H., and Zhang, H. (2014). The tumor necrosis factor receptor-associated factor (TRAF)-like family protein SEVEN IN ABSENTIA 2 (SINA2) promotes drought tolerance in an ABA-dependent manner in *Arabidopsis*. *New Phytol.* 202, 174–187.
- Belkhadir, Y., and Jallais, Y. (2015). The molecular circuitry of brassinosteroid signaling. *New Phytol.* 206, 522–540.
- Benjamini, Y., and Hochberg, Y. (1995). Controlling the false discovery rate—a practical and powerful approach to multiple testing. *J. Roy Stat. Soc. B Met.* 57, 289–300.
- Chalkley, R.J., and Clauser, K.R. (2012). Modification site localization scoring: strategies and performance. *Mol. Cell. Proteomics* 11, 3–14.
- Charrier, B., Champion, A., Henry, Y., and Kreis, M. (2002). Expression profiling of the whole *Arabidopsis* shaggy-like kinase multigene family by real-time reverse transcriptase-polymerase chain reaction. *Plant Physiol.* 130, 577–590.
- Chung, T., Phillips, A.R., and Vierstra, R.D. (2010). ATG8 lipidation and ATG8-mediated autophagy in *Arabidopsis* require ATG12 expressed from the differentially controlled ATG12A AND ATG12B loci. *Plant J.* 62, 483–493.
- Ciuffa, R., Lamark, T., Tarafder, A.K., Guesdon, A., Rybina, S., Hagen, W.J.H., Johansen, T., and Sachse, C. (2015). The selective autophagy receptor p62 forms a flexible filamentous helical scaffold. *Cell Rep.* 11, 748–758.
- Claeys, H., and Inze, D. (2013). The agony of choice: how plants balance growth and survival under water-limiting conditions. *Plant Physiol.* 162, 1768–1779.

- Clough, S.J., and Bent, A.F. (1998). Floral dip: a simplified method for *Agrobacterium*-mediated transformation of *Arabidopsis thaliana*. *Plant J.* 16, 735–743.
- Clouse, S.D. (2011). Brassinosteroid signal transduction: from receptor kinase activation to transcriptional networks regulating plant development. *Plant Cell* 23, 1219–1230.
- Contento, A.L., Kim, S.J., and Bassham, D.C. (2004). Transcriptome profiling of the response of *Arabidopsis* suspension culture cells to Suc starvation. *Plant Physiol.* 135, 2330–2347.
- Dal Santo, S., Stampfli, H., Krasensky, J., Kempa, S., Gibon, Y., Petutschnig, E., Rozhon, W., Heuck, A., Clausen, T., and Jonak, C. (2012). Stress-induced GSK3 regulates the redox stress response by phosphorylating glucose-6-phosphate dehydrogenase in *Arabidopsis*. *Plant Cell* 24, 3380–3392.
- Doelling, J.H., Walker, J.M., Friedman, E.M., Thompson, A.R., and Vierstra, R.D. (2002). The APG8/12-activating enzyme APG7 is required for proper nutrient recycling and senescence in *Arabidopsis thaliana*. *J. Biol. Chem.* 277, 33105–33114.
- Droese, S., Bindseil, K.U., Bowman, E.J., Siebers, A., Zeeck, A., and Altendorf, K. (1993). Inhibitory effect of modified bafilomycins and concanamycins on P- and V-type adenosine triphosphatases. *Biochemistry* 32, 3902–3906.
- Farmer, L.M., Book, A.J., Lee, K.-H., Lin, Y.-L., Fu, H., and Vierstra, R.D. (2010). The RAD23 family provides an essential connection between the 26S proteasome and ubiquitylated proteins in *Arabidopsis*. *Plant Cell* 22, 124–142.
- Farre, J.C., Burkenroad, A., Burnett, S.F., and Subramani, S. (2013). Phosphorylation of mitophagy and pexophagy receptors coordinates their interaction with Atg8 and Atg11. *EMBO Rep.* 14, 441–449.
- Floyd, B.E., Morriss, S.C., MacIntosh, G.C., and Bassham, D.C. (2012). What to eat: evidence for selective autophagy in plants. *J. Integr. Plant Biol.* 54, 907–920.
- Funakoshi, M., Sasaki, T., Nishimoto, T., and Kobayashi, H. (2002). Budding yeast Dsk2p is a polyubiquitin-binding protein that can interact with the proteasome. *Proc. Natl. Acad. Sci. USA* 99, 745–750.
- Guo, H., Li, L., Ye, H., Yu, X., Algreen, A., and Yin, Y. (2009). Three related receptor-like kinases are required for optimal cell elongation in *Arabidopsis thaliana*. *Proc. Natl. Acad. Sci. USA* 106, 7648–7653.
- Guo, H., Li, L., Aluru, M., Aluru, S., and Yin, Y. (2013). Mechanisms and networks for brassinosteroid regulated gene expression. *Curr. Opin. Plant Biol.* 16, 545–553.
- Hanaoka, H., Noda, T., Shirano, Y., Kato, T., Hayashi, H., Shibata, D., Tabata, S., and Ohsumi, Y. (2002). Leaf senescence and starvation-induced chlorosis are accelerated by the disruption of an *Arabidopsis* autophagy gene. *Plant Physiol.* 129, 1181–1193.
- Hao, J., Yin, Y., and Fei, S.Z. (2013). Brassinosteroid signaling network: implications on yield and stress tolerance. *Plant Cell Rep.* 32, 1017–1030.
- Harb, A., Krishnan, A., Ambavaram, M.M., and Pereira, A. (2010). Molecular and physiological analysis of drought stress in *Arabidopsis* reveals early responses leading to acclimation in plant growth. *Plant Physiol.* 154, 1254–1271.
- He, J.X., Gendron, J.M., Yang, Y., Li, J., and Wang, Z.Y. (2002). The GSK3-like kinase BIN2 phosphorylates and destabilizes BZR1, a positive regulator of the brassinosteroid signaling pathway in *Arabidopsis*. *Proc. Natl. Acad. Sci. USA* 99, 10185–10190.
- Inoue, Y., Suzuki, T., Hattori, M., Yoshimoto, K., Ohsumi, Y., and Moriyasu, Y. (2006). AtATG genes, homologs of yeast autophagy genes, are involved in constitutive autophagy in *Arabidopsis* root tip cells. *Plant Cell Physiol.* 47, 1641–1652.
- Kalvari, I., Tsompanis, S., Mulakkal, N.C., Osgood, R., Johansen, T., Nezis, I.P., and Promponas, V.J. (2014). iLIR. *Autophagy* 10, 913–925.
- Katari, M.S., Nowicki, S.D., Aceituno, F.F., Nero, D., Kelfer, J., Thompson, L.P., Cabello, J.M., Davidson, R.S., Goldberg, A.P., Shasha, D.E., et al. (2010). VirtualPlant: a software platform to support systems biology research. *Plant Physiol.* 152, 500–515.
- Kim, B., Jeong, Y.J., Corvalan, C., Fujioka, S., Cho, S., Park, T., and Choe, S. (2014). Darkness and gulliver2/phyB mutation decrease the abundance of phosphorylated BZR1 to activate brassinosteroid signaling in *Arabidopsis*. *Plant J.* 77, 737–747.
- Kinoshita, E., Kinoshita-Kikuta, E., Takiyama, K., and Koike, T. (2006). Phosphate-binding tag, a new tool to visualize phosphorylated proteins. *Mol. Cell. Proteomics* 5, 749–757.
- Kisselev, A.F., van der Linden, W.A., and Overkleeft, H.S. (2012). Proteasome inhibitors: an expanding army attacking a unique target. *Chem. Biol.* 19, 99–115.
- Kraft, C., Peter, M., and Hofmann, K. (2010). Selective autophagy: ubiquitin-mediated recognition and beyond. *Nat. Cell Biol.* 12, 836–841.
- Lee, D.Y., and Brown, E.J. (2012). Ubiquilins in the crosstalk among proteolytic pathways. *Biol. Chem.* 393, 441–447.
- Lee, D.Y., Arnott, D., and Brown, E.J. (2013). Ubiquilin4 is an adaptor protein that recruits Ubiquilin1 to the autophagy machinery. *EMBO Rep.* 14, 373–381.
- Li, J., and Chory, J. (1997). A putative leucine-rich repeat receptor kinase involved in brassinosteroid signal transduction. *Cell* 90, 929–938.
- Li, J., and Jin, H. (2007). Regulation of brassinosteroid signaling. *Trends Plant Sci.* 12, 37–41.
- Li, J., and Nam, K.H. (2002). Regulation of brassinosteroid signaling by a GSK3/SHAGGY-like kinase. *Science* 295, 1299–1301.
- Li, J.M., Nam, K.H., Vafeados, D., and Chory, J. (2001). BIN2, a new brassinosteroid-insensitive locus in *Arabidopsis*. *Plant Physiol.* 127, 14–22.
- Li, L., Yu, X., Thompson, A., Guo, M., Yoshida, S., Asami, T., Chory, J., and Yin, Y. (2009). *Arabidopsis* MYB30 is a direct target of BES1 and cooperates with BES1 to regulate brassinosteroid-induced gene expression. *Plant J.* 58, 275–286.
- Lin, Y.L., Sung, S.C., Tsai, H.L., Yu, T.T., Radjacomare, R., Usharani, R., Fatimababy, A.S., Lin, H.Y., Wang, Y.Y., and Fu, H. (2011). The defective proteasome but not substrate recognition function is responsible for the null phenotypes of the *Arabidopsis* proteasome subunit RPN10. *Plant Cell* 23, 2754–2773.
- Liu, Y.M., Xiong, Y., and Bassham, D.C. (2009). Autophagy is required for tolerance of drought and salt stress in plants. *Autophagy* 5, 954–963.
- Liu, Y.M., Burgos, J.S., Deng, Y., Srivastava, R., Howell, S.H., and Bassham, D.C. (2012). Degradation of the endoplasmic reticulum by autophagy during endoplasmic reticulum stress in *Arabidopsis*. *Plant Cell* 24, 4635–4651.
- Liu, X.D., Yao, J., Tripathi, D.N., Ding, Z., Xu, Y., Sun, M., Zhang, J., Bai, S., German, P., Hoang, A., et al. (2014). Autophagy mediates HIF2alpha degradation and suppresses renal tumorigenesis. *Oncogene* 34, 2450–2460.
- Lopez-Maury, L., Marguerat, S., and Bahler, J. (2008). Tuning gene expression to changing environments: from rapid responses to evolutionary adaptation. *Nat. Rev. Genet.* 9, 583–593.
- Maere, S., Heymans, K., and Kuiper, M. (2005). BiNGO: a cytoscape plugin to assess overrepresentation of Gene Ontology categories in Biological Networks. *Bioinformatics* 21, 3448–3449.
- Marshall, R.S., Li, F., Gemperline, D.C., Book, A.J., and Vierstra, R.D. (2015). Autophagic degradation of the 26S proteasome is mediated by the dual ATG8/ubiquitin receptor RPN10 in *Arabidopsis*. *Mol. Cell.* 58, 1053–1066.
- Maruyama, K., Takeda, M., Kidokoro, S., Yamada, K., Sakuma, Y., Urano, K., Fujita, M., Yoshiwara, K., Matsukura, S., Morishita, Y., et al. (2009). Metabolic pathways involved in cold acclimation identified by integrated analysis of metabolites and transcripts regulated by DREB1A and DREB2A. *Plant Physiol.* 150, 1972–1980.
- Michaeli, S., Galili, G., Genschik, P., Fernie, A.R., and Avin-Wittenberg, T. (2016). Autophagy in plants—what's new on the menu? *Trends Plant Sci.* 21, 134–144.
- Petherick, K.J., Williams, A.C., Lane, J.D., Ordonez-Moran, P., Huelsken, J., Collard, T.J., Smartt, H.J., Batson, J., Malik, K., Paraskeva, C., et al. (2013). Autolysosomal beta-catenin degradation regulates Wnt-autophagy-p62 crosstalk. *EMBO J.* 32, 1903–1916.
- Pratelli, R., Guerra, D.D., Yu, S., Wogulis, M., Kraft, E., Frommer, W.B., Callis, J., and Pilot, G. (2012). The ubiquitin E3 ligase LOSS OF GDU2 is required for

- GLUTAMINE DUMPER1-induced amino acid secretion in *Arabidopsis*. *Plant Physiol.* 158, 1628–1642.
- Pryor, K.D., and Leiting, B. (1997). High-level expression of soluble protein in *Escherichia coli* using a His(6)-tag and maltose-binding-protein double-affinity fusion system. *Protein Expr. Purif.* 10, 309–319.
- Qin, F., Sakuma, Y., Tran, L.S., Maruyama, K., Kidokoro, S., Fujita, Y., Fujita, M., Umezawa, T., Sawano, Y., Miyazono, K., et al. (2008). *Arabidopsis* DREB2A-interacting proteins function as RING E3 ligases and negatively regulate plant drought stress-responsive gene expression. *Plant Cell* 20, 1693–1707.
- Ren, M., Qiu, S., Venglat, P., Xiang, D., Feng, L., Selvaraj, G., and Datla, R. (2011). Target of rapamycin regulates development and ribosomal RNA expression through kinase domain in *Arabidopsis*. *Plant Physiol.* 155, 1367–1382.
- Sakuma, Y., Maruyama, K., Osakabe, Y., Qin, F., Seki, M., Shinozaki, K., and Yamaguchi-Shinozaki, K. (2006). Functional analysis of an *Arabidopsis* transcription factor, DREB2A, involved in drought-responsive gene expression. *Plant Cell* 18, 1292–1309.
- Skirycz, A., Vandenbroucke, K., Clauw, P., Maleux, K., De Meyer, B., Dhondt, S., Pucci, A., Gonzalez, N., Hoerberichts, F., Tognetti, V.B., et al. (2011). Survival and growth of *Arabidopsis* plants given limited water are not equal. *Nat. Biotechnol.* 29, 212–214.
- Sun, Y., Fan, X.-Y., Cao, D.-M., Tang, W., He, K., Zhu, J.-Y., He, J.-X., Bai, M.-Y., Zhu, S., Oh, E., et al. (2010). Integration of brassinosteroid signal transduction with the transcription network for plant growth regulation in *Arabidopsis*. *Dev. Cell* 19, 765–777.
- Svenning, S., Lamark, T., Krause, K., and Johansen, T. (2011). Plant NBR1 is a selective autophagy substrate and a functional hybrid of the mammalian autophagic adapters NBR1 and p62/SQSTM1. *Autophagy* 7, 993–1010.
- Thompson, A.R., Doelling, J.H., Sutangkakul, A., and Vierstra, R.D. (2005). Autophagic nutrient recycling in *Arabidopsis* directed by the ATG8 and ATG12 conjugation pathways. *Plant Physiol.* 138, 2097–2110.
- Urao, T., Yamaguchi-Shinozaki, K., Urao, S., and Shinozaki, K. (1993). An *Arabidopsis* myb homolog is induced by dehydration stress and its gene product binds to the conserved MYB recognition sequence. *Plant Cell* 5, 1529–1539.
- Vierstra, R.D. (2009). The ubiquitin-26S proteasome system at the nexus of plant biology. *Nat. Rev. Mol. Cell Biol.* 10, 385–397.
- Villarasa-Blasi, J., Gonzalez-Garcia, M.P., Frigola, D., Fabregas-Vallve, N., Alexiou, K.G., Lopez-Bigas, N., Rivas, S., Jauneau, A., Lohmann, J.U., Benfey, P.N., et al. (2015). Regulation of plant stem cell quiescence by a brassinosteroid signaling module. *Dev. Cell* 33, 238.
- Wang, Z.Y., Nakano, T., Gendron, J., He, J.X., Chen, M., Vafeados, D., Yang, Y.L., Fujioka, S., Yoshida, S., Asami, T., et al. (2002). Nuclear-localized BZR1 mediates brassinosteroid-induced growth and feedback suppression of brassinosteroid biosynthesis. *Dev. Cell* 2, 505–513.
- Wang, Y., Sun, S., Zhu, W., Jia, K., Yang, H., and Wang, X. (2013). Strigolactone/MAX2-induced degradation of brassinosteroid transcriptional effector BES1 regulates shoot branching. *Dev. Cell* 27, 681–688.
- Wang, X., Chen, J., Xie, Z., Liu, S., Nolan, T., Ye, H., Zhang, M., Guo, H., Schnable, P.S., Li, Z., et al. (2014). Histone lysine methyltransferase SDG8 is involved in brassinosteroid-regulated gene expression in *Arabidopsis thaliana*. *Mol. Plant* 7, 1303–1315.
- Weber, C., Nover, L., and Fauth, M. (2008). Plant stress granules and mRNA processing bodies are distinct from heat stress granules. *Plant J.* 56, 517–530.
- Wild, P., Farhan, H., McEwan, D.G., Wagner, S., Rogov, V.V., Brady, N.R., Richter, B., Korac, J., Waidmann, O., Choudhary, C., et al. (2011). Phosphorylation of the autophagy receptor optineurin restricts salmonella growth. *Science* 333, 228–233.
- Wu, T.D., and Nacu, S. (2010). Fast and SNP-tolerant detection of complex variants and splicing in short reads. *Bioinformatics* 26, 873–881.
- Wu, F.-H., Shen, S.-C., Lee, L.-Y., Lee, S.-H., Chan, M.-T., and Lin, C.-S. (2009). Tape-*Arabidopsis* Sandwich - a simpler *Arabidopsis* protoplast isolation method. *Plant Methods* 5, 16.
- Yang, X., and Bassham, D.C. (2015). New insight into the mechanism and function of autophagy in plant cells. *Int. Rev. Cell Mol. Biol.* 320, 1–40.
- Yan, Z.Y., Zhao, J., Peng, P., Chihara, R.K., and Li, J.M. (2009). BIN2 functions redundantly with other *Arabidopsis* GSK3-like kinases to regulate brassinosteroid signaling. *Plant Physiol.* 150, 710–721.
- Yin, Y.H., Wang, Z.Y., Mora-Garcia, S., Li, J.M., Yoshida, S., Asami, T., and Chory, J. (2002). BES1 accumulates in the nucleus in response to brassinosteroids to regulate gene expression and promote stem elongation. *Cell* 109, 181–191.
- Yin, Y., Vafeados, D., Tao, Y., Yoshida, S., Asami, T., and Chory, J. (2005). A new class of transcription factors mediates brassinosteroid-regulated gene expression in *Arabidopsis*. *Cell* 120, 249–259.
- Yoo, S.D., Cho, Y.H., and Sheen, J. (2007). *Arabidopsis* mesophyll protoplasts: a versatile cell system for transient gene expression analysis. *Nat. Protoc.* 2, 1565–1572.
- Yoshimoto, K., Hanaoka, H., Sato, S., Kato, T., Tabata, S., Noda, T., and Ohsumi, Y. (2004). Processing of ATG8s, ubiquitin-like proteins, and their deconjugation by ATG4s are essential for plant autophagy. *Plant Cell* 16, 2967–2983.
- Youn, J.H., and Kim, T.W. (2015). Functional insights of plant GSK3-like kinases: multi-taskers in diverse cellular signal transduction pathways. *Mol. Plant* 8, 552–565.
- Yu, X., Li, L., Li, L., Guo, M., Chory, J., and Yin, Y. (2008). Modulation of brassinosteroid-regulated gene expression by jumonji domain-containing proteins ELF6 and REF6 in *Arabidopsis*. *Proc. Natl. Acad. Sci. USA* 105, 7618–7623.
- Yu, X., Li, L., Zola, J., Aluru, M., Ye, H., Foudree, A., Guo, H., Anderson, S., Aluru, S., Liu, P., et al. (2011). A brassinosteroid transcriptional network revealed by genome-wide identification of BES1 target genes in *Arabidopsis thaliana*. *Plant J.* 65, 634–646.
- Zhang, S., Cai, Z., and Wang, X. (2009). The primary signaling outputs of brassinosteroids are regulated by abscisic acid signaling. *Proc. Natl. Acad. Sci. USA* 106, 4543–4548.
- Zhang, Y., Liu, Z., Wang, J., Chen, Y., Bi, Y., and He, J. (2015). Brassinosteroid is required for sugar promotion of hypocotyl elongation in *Arabidopsis* in darkness. *Planta* 242, 881–893.
- Zhang, Z., Zhu, J.Y., Roh, J., Marchive, C., Kim, S.K., Meyer, C., Sun, Y., Wang, W., and Wang, Z.Y. (2016). TOR signaling promotes accumulation of BZR1 to balance growth with carbon availability in *Arabidopsis*. *Curr. Biol.* 26, 1854–1860.
- Zhao, J., Peng, P., Schmitz, R.J., Decker, A.D., Tax, F.E., and Li, J. (2002). Two putative BIN2 substrates are nuclear components of brassinosteroid signaling. *Plant Physiol.* 130, 1221–1229.
- Zhou, J., Wang, J., Cheng, Y., Chi, Y.J., Fan, B., Yu, J.Q., and Chen, Z. (2013). NBR1-mediated selective autophagy targets insoluble ubiquitinated protein aggregates in plant stress responses. *PLoS Genet.* 9, e1003196.
- Zhu, Y., Massen, S., Terenzio, M., Lang, V., Chen-Lindner, S., Eils, R., Novak, I., Dikic, I., Hamacher-Brady, A., and Brady, N.R. (2013). Modulation of serines 17 and 24 in the LC3-interacting region of Bnip3 determines pro-survival mitophagy versus apoptosis. *J. Biol. Chem.* 288, 1099–1113.

STAR★METHODS**KEY RESOURCES TABLE**

REAGENT or RESOURCE	SOURCE	IDENTIFIER
Antibodies		
Rabbit polyclonal anti-BES1	(Yu et al., 2011)	N/A
Rabbit polyclonal anti-HERK1	(Guo et al., 2009)	N/A
Rabbit polyclonal anti-DSK2	(Lin et al., 2011)	N/A
Rabbit polyclonal anti-GFP	This study	N/A
Rabbit polyclonal anti-c-MYC	Sigma-Aldrich	Cat#C3956; RRID: AB_439680
Rabbit polyclonal anti-IWS1	This study	N/A
Chicken polyclonal anti-Ubiquitin	(Pratelli et al., 2012)	N/A
Mouse monoclonal anti-MBP	New England Biolabs	Cat#E8032S; RRID: AB_1559732
Mouse monoclonal anti-Tubulin	Sigma-Aldrich	Cat#T8203; RRID: AB_1841230
Mouse monoclonal anti-c-MYC	Cell Signaling Technology	Cat#2278S; RRID: AB_10693332
Chemicals, Peptides, and Recombinant Proteins		
MG132	Sigma-Aldrich	Cat#M7449
Concanamycin A	Sigma-Aldrich	Cat#C9705
E64d	Sigma-Aldrich	Cat#E8940
Mannitol	Sigma-Aldrich	Cat#M4125
Cycloheximide	Sigma-Aldrich	Cat#C4859
Brassinazole	Tadao Asami (Asami et al., 2000)	N/A
TUBE2 Agarose	LifeSensors	Cat#UM402
Phos-tag	Wako	Cat#AAL-107
Complete protease inhibitor cocktail tablets	Roche	Cat#11836170001
Trizol	Thermo Fisher	Cat#15596018
RNeasy Kit	Qiagen	Cat# 74904
Glu-C	Thermo Fisher	Cat#90054
Trypsin	Roche	Cat# 03708969001
Linsmaier and Skoog	Caisson Laboratories	Cat#LSP03-1LT
Deposited Data		
Raw mass spectra	MassIVE repository	MassIVE ID: MSV000079641
Raw data files for DNA sequencing	NCBI Gene Expression Omnibus	GEO: GSE93420
Experimental Models: Organisms/Strains		
<i>E. coli</i> BL21 Gold (DE3)	Thermo Fisher	Cat#50-125-348
<i>Agrobacterium tumefaciens</i> (strain GV3101)		N/A
<i>Arabidopsis thaliana</i> : WT Col-0		N/A
<i>Arabidopsis thaliana</i> : <i>atg5-1</i>	(Thompson et al., 2005)	N/A
<i>Arabidopsis thaliana</i> : <i>atg7-2</i>	(Chung et al., 2010)	N/A
<i>Arabidopsis thaliana</i> : <i>bri1-301</i>	(Li and Nam, 2002)	N/A
<i>Arabidopsis thaliana</i> : <i>bes1-D</i>	(Vilarrasa-Blasi et al., 2015; Yin et al., 2002)	N/A
<i>Arabidopsis thaliana</i> : <i>bin2-1D</i>	(Li et al., 2001)	N/A
<i>Arabidopsis thaliana</i> : <i>bin2-3 bil1 bil2</i>	(Yan et al., 2009)	N/A
<i>Arabidopsis thaliana</i> : <i>BES1P-BES1-GFP</i>	(Yin et al., 2002)	N/A
<i>Arabidopsis thaliana</i> : <i>DSK2-RNAi 2-6</i>	(Lin et al., 2011)	N/A
<i>Arabidopsis thaliana</i> : <i>DSK2-RNAi 1-4</i>	(Lin et al., 2011)	N/A
<i>Arabidopsis thaliana</i> : <i>SINAT RNAi #5</i>	(Yang et al., 2017)	N/A
<i>Arabidopsis thaliana</i> : <i>SINAT RNAi #14</i>	(Yang et al., 2017)	N/A

(Continued on next page)

Continued

REAGENT or RESOURCE	SOURCE	IDENTIFIER
<i>Arabidopsis thaliana</i> : DSK2A ^D -MYC-1	This study	N/A
<i>Arabidopsis thaliana</i> : DSK2A ^D -MYC-2	This study	N/A
<i>Arabidopsis thaliana</i> : DSK2A ^A -MYC-1	This study	N/A
<i>Arabidopsis thaliana</i> : DSK2A ^A -MYC-2	This study	N/A
<i>Arabidopsis thaliana</i> : DSK2A ^{mAIM} -MYC-1	This study	N/A
<i>Arabidopsis thaliana</i> : DSK2A ^{mAIM} -MYC-2	This study	N/A
<i>Arabidopsis thaliana</i> : DSK2A-GFP	This study	N/A
Recombinant DNA		
pET42a GST	Novagen	Cat#70561
pET42a GST-DSK2A	This study	N/A
pET42a GST-DSK2B	This study	N/A
pET42a GST-ATG8a	This study	N/A
pET42a GST-ATG8e	This study	N/A
pET42a GST-ATG8f	This study	N/A
pET42a GST-ATG8i	This study	N/A
pET42a GST-BIN2	(Yin et al., 2002)	N/A
pET28a HIS-DSK2A	This study	N/A
pETMALc-H MBP	Pryor and Leiting, 1997	N/A
pETMBP-H	This study	N/A
pETMALc-H MBP-BES1	(Yin et al., 2002)	N/A
pETMALc-H MBP-SINAT2	This study	N/A
pETMALc-H MBP-BIN2	(Yin et al., 2002)	N/A
pETMBP-H MBP-DSK2A	This study	N/A
pETMBP-H MBP-DSK2A C1 (AA 90-538)	This study	N/A
pETMBP-H MBP-DSK2A C2 (AA 403-538)	This study	N/A
pGBK7	TAKARA	Cat#630443
pGADT7	TAKARA	Cat#630442
pGADT7 BES1	(Yin et al., 2002)	N/A
pGADT7 BIN2	(Yin et al., 2002)	N/A
pGADT7 DSK2A	This study	N/A
pGADT7 ATG8e	This study	N/A
pGBK7 DSK2A	This study	N/A
pGBK7 DSK2A ^D	This study	N/A
pGBK7 DSK2A ^A	This study	N/A
pGBK7 DSK2A ^{mAIM}	This study	N/A
pGBK7 DSK2A ^A mAIM	This study	N/A
pGBK7 DSK2A ^{D12}	This study	N/A
pGBK7 DSK2A ^{A12}	This study	N/A
pYY46 35S:BES1-GFP	(Yin et al., 2002)	N/A
pYY46 35S:DSK2-GFP	This study	N/A
pXY136 35S:BES1-YFP	This study	N/A
pLZ0102 35S:BIN2-1D-YFP	This study	N/A
pPZP211-BES1P:BES1-GFP	(Yin et al., 2002)	N/A
pPZP211-35S:Cerulean-ATG8e	This study	N/A
pAN578 35S:Cerulean-ATG8e	(Liu et al., 2012)	N/A
pYY361 BRI1P: DSK2A ^D -MYC	This study	N/A
pYY361 BRI1P: DSK2A ^A -MYC	This study	N/A
pYY361 BRI1P: DSK2A ^{mAIM} -MYC	This study	N/A
pXY103 35S:YFPN	(Yu et al., 2008)	N/A

(Continued on next page)

Continued

REAGENT or RESOURCE	SOURCE	IDENTIFIER
pXY104 35S:YFPC	(Yu et al., 2008)	N/A
pXY103 35S:BES1-YFPN	(Wang et al., 2014)	N/A
pXY103 35S:DSK2A-YFPN	This study	N/A
pXY103 35S: DSK2A ^D -YFPN	This study	N/A
pXY103 35S: DSK2A ^{mAIM} -YFPN	This study	N/A
pXY103 35S:BIN2-YFPN	This study	N/A
pXY104 35S:DSK2A-YFPC	This study	N/A
pXY104 35S:DSK2A ΔUBA-YFPC	This study	N/A
pXY104 35S:DSK2B-YFPC	This study	N/A
pXY104 35S:ATG8e-YFPC	This study	N/A
pXY104 35S:SINAT2-YFPC	This study	N/A
Oligonucleotides		
Full list of DSK2A variants is presented in Table S4		
Full list of primers is presented in Table S5		
Software and Algorithms		
R statistical package	www.r-project.org	ver 3.3.0; SCR_001905
JMP Pro	www.jmp.com	ver 12

CONTACT FOR REAGENT AND RESOURCE SHARING

Further information and requests for reagents may be directed to and will be fulfilled by the Lead Contact, Yanhai Yin (yin@iastate.edu).

EXPERIMENTAL MODEL AND SUBJECT DETAILS**Plant Materials and Growth Conditions**

Arabidopsis thaliana accession Columbia (Col-0) was used along with previously described mutants: *atg5-1* (Thompson et al., 2005), *atg7-2* (Chung et al., 2010), *bri1-301* (Li and Nam, 2002), *bes1-D* (Vilarrasa-Blasi et al., 2015; Yin et al., 2002), *bin2-1D* (Li et al., 2001), *bin2-3 bil1 bil2* (Yan et al., 2009). Well characterized DSK2 RNAi lines (Lin et al., 2011) were used in this study. The majority of experiments in this manuscript were conducted with DSK2 RNAi 2-6 (referred to as DSK2 RNAi) and another independent line (DSK2 RNAi 1-4) was used to verify the phenotype. DSK2 RNAi BES1 RNAi plants were generated by crossing DSK2 RNAi with BES1 RNAi and F1 progeny used to examine BES1 and DSK2 protein levels as well as drought phenotypes. Plants were grown on 0.5X Linsmaier and Skoog (LS; Caisson Laboratories) plates or in soil under long day (16 h light/8 h dark) conditions at 22°C unless otherwise specified.

METHOD DETAILS**Inhibitor Treatments**

Treatment with proteasome or autophagy inhibitors was performed by soaking plants in 0.5X LS liquid medium containing DMSO, 50 μM MG132, 20 μM E64d or 1 μM ConA. Plants were vacuum infiltrated for 5 minutes and then kept under light for 6 hours before sample collection. Similarly, cycloheximide treatments were performed by soaking plants in 0.5X LS medium containing 500 μM cycloheximide for the indicated time points. For BES1 ubiquitination, BES1-YFP was expressed in *N. benthamiana*. 24 hours post-inoculation, infiltration medium (10 mM MgCl₂, 10 mM MES, pH 5.7) containing DMSO, 50 μM MG132, or 20 μM E64d was infiltrated into the lower side of the leaves. Samples were collected 16 hours after addition of inhibitors.

BRZ Response Assays

For BRZ response assays under normal (non-stressed) conditions, sterilized seeds were planted directly on 0.5X LS medium with 1% sucrose containing DMSO or indicated concentrations of BRZ (Asami et al., 2000). Plates were exposed to light for 6-8 hours and then kept in darkness for 7 days. Seedlings were then imaged and hypocotyls quantified using ImageJ software (<http://imagej.nih.gov/ij/>). For BRZ response under stress conditions, seedlings were grown under light for 5 days on 0.5X LS medium and then transferred to medium containing DMSO or 1 μM BRZ in combination with control (+ suc; containing 1% sucrose), starvation (without sucrose) or mannitol (350 mM mannitol) stresses. The seedlings were incubated in darkness for 3 days following transfer and then hypocotyl length was quantified as described above.

Drought and Dehydration Assays

Drought survival assays were performed by withholding water for 2-3 weeks to impose drought stress followed by rewetting. 7 days after rewetting plants were scored for survival as judged by the presence of new green leaves. Equal water and soil amounts were assured in drought assays by weighing the amount of dry soil for each pot and watering with equal amounts of water. Pots were randomized in trays to control for varying water loss due to position. Dehydration treatments were performed as previously described (Qin et al., 2008). Briefly, whole rosettes of 4-week-old plants were removed from pots and placed in empty petri dishes (dehydration) or in petri dishes containing moistened kimwipes (mock control) and sealed with parafilm for 4 hours. Detached leaf water loss assays were performed with 4-5 week old plants grown under short day conditions as previously described (Bao et al., 2014).

Fixed-Carbon Starvation Assays

Fixed-carbon starvation survival assays in seedlings were performed as described by (Chung et al., 2010). Seedlings were grown on 0.5X LS plates without sucrose in light for one week and then transferred to darkness for 8-12 days as indicated. After dark treatment, the seedlings were placed back in light conditions for one week. Plants with new growth were counted as surviving. For fixed-carbon starvation treatments of plants in soil, plants were grown for 4-5 weeks under short day conditions and then transferred to a dark chamber at 22°C. After 8 or 9 days dark incubation, plants were transferred back into light for one week recovery before being scored for survival.

Immunoprecipitation

The majority of immunoprecipitation experiments were carried out as follows: plant leaf tissue was ground to a fine powder and re-suspended in 2-3 volumes of protein extraction buffer. Extracts were then filtered through Miracloth (Calbiochem), and insoluble debris removed by centrifugation for 10 minutes at 5000 g, 4°C. The protein extracts were incubated for 2-4 hours with GFP-trap agarose beads (Chromotek) or with anti-GFP antibody followed by Protein-A agarose beads (Pierce). Beads were then washed 3-5 times with protein extraction buffer containing 0.1%-0.5% Triton X-100 and eluted by boiling in 2X SDS sample buffer. CIP treatments were performed at 37 degrees for one hour using Alkaline phosphatase (Roche) as described (Yin et al., 2002). Cerulean-ATG8 was Immunoprecipitated from the membrane fraction by grinding 5 g fresh *N. benthamiana* tissue (48 hours post-inoculation) in 20 mL cold extraction buffer (0.3 M Sucrose, 0.1 M Tris-HCl, pH7.5, 1 mM EDTA, 1 mM PMSF). The extract was then passed through Miracloth (Calbiochem) and centrifuged for 5 minutes at 1,000 g, 4°C to remove insoluble material. The supernatant was then centrifuged at 100,000 g for 30 minutes, 4°C. The membrane pellet was resuspended in Phosphate buffered saline (PBS) supplemented with 1% Triton X-100, 10 mM Beta-mercaptoethanol and Roche complete mini protease inhibitor cocktail by gentle rocking for 2 hours at 4°C. The extract was centrifuged again at 100,000 g for 30 minutes, 4°C and the supernatant was incubated with 20 µL GFP-Trap agarose beads (Chromotek) overnight. Beads were then washed 5 times with PBS containing 0.1% Triton X-100 and eluted by boiling in 2X SDS sample buffer.

TUBE Ubiquitination Assays

To detect BES1 ubiquitination, Tandem Ubiquitin Binding Entities (TUBEs; LifeSensors) were used to enrich total ubiquitinated proteins. Harvested tissue was ground to a fine powder in liquid nitrogen and extracted in protein extraction buffer (50 mM Tris-Cl, pH 7.4, 150 mM NaCl, 10% glycerol) supplemented with complete mini protease inhibitor cocktail (Roche) and deubiquitinase inhibitor (50 µM PR-619; LifeSensors). Extract was clarified by two rounds of centrifugation at 13,000 g for 10 minutes at 4°C and the supernatant was incubated with blocked agarose (control) or TUBE2 agarose beads for 3 hours with gentle rocking at 4°C. Beads were then washed 4 times with protein extraction buffer and eluted by boiling in 2X SDS sample buffer.

Western Blotting

Protein was extracted in protein extraction buffer (50 mM Tris-Cl, pH 7.4, 150 mM NaCl, 10% glycerol) supplemented with complete mini protease inhibitor cocktail (Roche) followed by quantification using Bradford assay or by fresh weight through directly adding 2-3 volumes of 2X SDS sample buffer to ground plant tissue. Western blotting was performed using standard laboratory techniques. Phos-tag SDS-PAGE was conducted by adding 1 mM MnCl₂ to protein samples and running SDS-PAGE gels containing 100 µM Phos-tag reagent (Wako) according to the manufacturer's instructions. The following antibodies were used in this study in conjunction with appropriate secondary antibody-HRP conjugates : anti-BES1 (Yu et al., 2011), anti-DSK2 (Lin et al., 2011), anti-HERK1 (Guo et al., 2009), anti-GFP, anti-Tubulin (Sigma), anti-Ubiquitin (Pratelli et al., 2012), anti-MYC (Sigma or Cell Signaling Technology), anti-MBP (NEB).

RNA-Seq

RNA-seq experiments were performed using 4-week old plants under control, 4 hour dehydration, or 5 days dark treatment for starvation. 3 biological replicates were performed for control and dehydration conditions and 2 biological replicates for starvation. For each replicate, whole rosette tissue from 3-4 plants was pooled. RNA was then extracted using Trizol, followed by DNAse digestion and RNA cleanup using Qiagen RNeasy kit. Purified RNA was subject to quality control on an Agilent 2100 Bioanalyzer. Library preparation and RNA sequencing were performed by BGI Americas using an Illumina HiSeq 2000 with 50bp single-end reads and ~30 million reads per sample. Details of data processing and statistical analysis of RNA-seq data are provided in the Quantification and Statistical Analysis section.

Yeast-Two Hybrid

Yeast-two hybrid screening for BES1 interacting proteins using the Clontech matchmaker system was described previously (Yin et al., 2005). DSK2A was recovered from a screen using BES1-N domain as bait (amino acid residues 1–99) and SINAT2 was recovered using BES1-P domain (amino acid residues 100–150). For pairwise yeast-two hybrid assays, full length BES1, ATG8e, BIN2 and DSK2 were cloned into GBKT7 or GADT7 vectors and transformed into yeast strain Y187. Yeast cells were grown in medium lacking Trp and Leu and assayed for LacZ activity as described in the Yeast Protocols Handbook (Clontech) using X-gal (5-bromo-4-chloro-3-indolyl-b-D-galactopyranoside).

In Vitro Pull-down Assays

For GST-pull-down assays, GST or MBP fusions were generated by cloning into pET42a, pET-MALc-H or pET-MBP-H vectors. DSK2A-HIS fusion protein constructs were generated by cloning DSK2A into pET28a. Recombinant proteins were produced in *E. coli* strain BL21, and tested for interaction as described previously (Yin et al., 2002). GST or each GST tagged fusion were incubated with indicated MBP fusion proteins in 1 mL GST-pull-down buffer (50 mM Tris-HCl pH 7.5, 200 mM NaCl, 0.5% Triton X-100 and 0.5 mM Beta-mercaptoethanol, Roche complete mini protease inhibitor cocktail) at room temperature for 2 hours on a tube rotator. Following incubation, 20 μL GST beads pre-blocked overnight with 1 mg/mL BSA and BL21 extract were added and the incubation was continued for an additional 30 minutes. GST beads were washed in GST-pull-down buffer 5–6 times and then eluted in 2X SDS sample buffer. For pull-down reactions exhibiting high background, an alternative pull-down buffer was substituted (25 mM HEPES-KOH [pH 8.0], 1 mM DTT, 50 mM KCl, 10% glycerol and 1% NP-40). GST-pull-down experiments were repeated 2–3 times with similar results. For pull-down of DSK2A-HIS, phosphorylated BES1-MBP protein was generated by incubating BES1-MBP with BIN2-GST in kinase buffer containing 10 mM ATP (rotated 5 hours at 37 degrees). Non-phosphorylated BES1 control was produced with an identical reaction lacking ATP. Pull-down assays were carried out as described above, except that blocked amylose resin (NEB) was used to capture the MBP proteins. DSK2A-HIS was detected with anti-DSK2 antibodies.

BiFC Assays

BiFC assays were conducted using constructs for the N- or C-terminus of YFP (Yu et al., 2008). BES1, DSK2, ATG8e, BIN2, and SINAT2 were cloned upstream of YFP fragments and transformed into *Agrobacterium tumefaciens* (strain GV3101). *Agrobacterium* cultures were grown overnight in LB medium containing 200 mM acetosyringone, washed with infiltration medium (10 mM MgCl₂, 10 mM MES, pH 5.7, 200 mM acetosyringone) and resuspended to an OD600 of 1.0. *Agrobacterium* carrying NYFP and CYFP constructs were mixed in equal ratios, and the *Agrobacterium* mixtures were infiltrated into the lower surface of *N. benthamiana* leaves. After 36–48 hours, YFP signal was detected using a Leica SP5 X MP confocal microscope equipped with an HCS PL APO CS 20.0×0.70 oil objective. YFP was excited with a 514-nm laser line and detected from 530 to 560 nm. Images were acquired with LAS AF software (Leica Microsystems) using identical settings for samples and controls. For BiFC colocalization studies, *Agrobacterium* carrying Cerulean-ATG8e was mixed along with NYFP and CYFP constructs at equal ratios and infiltrated into *N. benthamiana* as described above. Confocal microscopy was used to image YFP and CFP sequentially to reduce cross-excitation. YFP was excited with a 514 nm laser line and detected from 530–560 nm. CFP was excited at 405 nm and detected from 460–490 nm. BiFC experiments were repeated 2–3 times.

Coexpression of DSK2 and BIN2 in Tobacco

DSK2-MYC or DSK2 A-MYC (containing putative BIN2 phosphorylation sites mutated to alanine) was co-expressed with BIN2-D-YFP (bin2-1) (Li et al., 2001) or empty YFP vector in *N. benthamiana* as described for BiFC assays. Leaf tissue was collected for protein extraction 2 days post-infiltration.

Plasmid Constructs and Generation of Transgenic Plants

Plasmid constructs were generated using standard laboratory techniques via restriction enzyme digestion or Gateway technology (Invitrogen) and were confirmed by DNA sequencing. pET-MBP-H vector was generated by modifying pETMALc-H (Pryor and Leiting, 1997) via digestion with SacI and Xhol and replacement of the multiple cloning site with a redesigned sequence (GAGCTCCNGC GAATTACGGGATCCCTGGGTACCCGCAAGCTTCGAGTCGACTACCTCGAG). gBlocks gene synthesis (IDT) was used to generate DSK2 mutants. An overview of mutated DSK2 sites and oligonucleotides used in this study is provided (Tables S4 and S5). DSK2-MYC constructs were generated by fusing DSK2 or mutated DSK2 variants with a C-terminal 2X MYC tag driven by the strong constitutive BRI1 promoter (Li et al., 2009; Li and Chory, 1997). Plasmid constructs were transferred into *Agrobacterium tumefaciens* (strain GV3101) and used to transform plants by the floral-dip method (Clough and Bent, 1998). Transgenic plants were screened on 0.5X LS plates supplemented with 50 mg/L kanamycin and further confirmed via western blotting using anti-MYC antibodies.

Protoplast Transient Expression Assays

Protoplasts were prepared from *Arabidopsis* rosette leaves grown under short day conditions and transformed using 30–50 μg of plasmid DNA via the PEG method (Wu et al., 2009; Yoo et al., 2007). Transformed protoplasts were incubated in darkness for 36–48 hours with control (+sucrose; 5% sucrose added), starvation (−sucrose; without sucrose) or mannitol (350 mM mannitol) treatments and concanamycin A (Sigma) or dimethyl sulfoxide (DMSO) were added 12 hours before visualization by confocal microscopy. Confocal microscopy was performed with a Leica (Leica Microsystems) SP5 X MP confocal microscope equipped with a resonance

scanner and HPX PL APO CS 63.0x1.40 oil objective. For colocalization assays, YFP and CFP were imaged sequentially to avoid cross-detection between channels. Excitation and detection wavelengths were the same as those described for BiFC colocalization assays.

Confocal Microscopy of *Arabidopsis* Roots

For imaging of BES1-GFP signal, homozygous BES1P:BES1-GFP lines were grown for 5 days in light and then transferred to –sucrose plates for 2-day starvation treatments. DMSO or 1 μ M conA was applied by transferring the plants to liquid 0.5X LS medium 16 hours prior to imaging. Confocal microscopy was performed with a Leica (Leica Microsystems) SP5 X MP confocal microscope equipped with a HCX PL APO CS 40.0x1.25 oil objective. GFP was excited with a 488 nm laser line and detected from 500–580 nm.

Phosphorylation Assays

For in vitro kinase assays, MBP or DSK2-MBP proteins were mixed with BIN2-HIS in 20 μ L kinase buffer (20 mM Tris, pH 7.5, 100 mM NaCl, 12 mM MgCl₂ and 10 μ Ci ³²P- γ ATP) as previously described (Yin et al., 2002). For Mass spectrometry analysis of phosphorylated proteins, DSK2-MBP was phosphorylated using BIN2-MBP in kinase buffer containing 20 mM ATP.

Protein Digestion and LC-MS/MS

Proteins were reduced with 5 mM TCEP in ammonium bicarbonate for 5 min at 94 °C. Proteins were then digested using either Glu-C (ThermoFisher) or trypsin (Roche) at 37 °C overnight and then alkylated with 12.5 mM iodacetamide for 15 min at 37 °C in the dark. Peptides were further digested using an additional aliquot of Glu-C or trypsin for 2 hrs. Samples were then acidified to a pH of ~3 with formic acid. Digested peptides were purified using Waters Oasis MCX cartridges and eluted using 45%IPA/500 mM NH₄HCO₃. Eluted peptides were dried using a speedvac (Thermo) and resuspended in 0.1% formic acid. Peptide amount was then quantified using the Pierce BCA Protein assay kit.

An Agilent 1260 quaternary HPLC was used to deliver a flow rate of ~600 nL min⁻¹ to a 3-phase capillary chromatography column through a splitter. The 3-phase capillary chromatography was assembled as follows. Using a Next Advance pressure cell a fused silica capillary column was packed with 5 mM Zorbax SB-C18 (Agilent) to form the first dimension reverse phase column (RP1). A 5 cm long strong cation exchange (SCX) column packed with 5 μ m PolySulfoethyl (PolyLC) was connected to RP1 using a zero dead volume 1 μ m filter (Upchurch, M548) attached to the exit of the RP1 column. A nanospray fused silica capillary was pulled to a sharp tip using a laser puller (Sutter P-2000) and packed with 2.5 μ m C18 (Waters) to form RP2 and then connected to the SCX column. The 3 sections were joined and mounted on a custom electrospray source for on-line nested elutions. A new set of columns was used for every sample. Peptides were loaded onto RP1 using the Next Advance pressure cell. Peptides were eluted from RP1 unto the SCX column using a 0 to 80% acetonitrile gradient over 60 min. Peptides were then fractionated using the SCX column using a series of 9 salt gradients (0, 30, 50, 60, 70, 80, 90, 100 and 1000 mM ammonium acetate), followed by high resolution reverse phase separation using an acetonitrile gradient of 0-80% for 150 min.

Spectra were acquired on a Thermo Scientific Q-Exactive high-resolution quadrupole Orbitrap mass spectrometer. Data dependent acquisition was obtained using Xcalibur 3.0.63 software in positive ion mode with a spray voltage of 2.00 kV and a capillary temperature of 275 °C. MS1 spectra were measured at a resolution of 70,000, an automatic gain control (AGC) of 3e6 with a maximum ion time of 100 ms and a mass range of 400-2000 m/z. Up to 15 MS2 were triggered at a resolution of 17,500, an AGC of 1e5 with a maximum ion time of 50 ms and a normalized collision energy of 28. MS1 that triggered MS2 scans were dynamically excluded for 15 s.

The raw data were extracted and searched using Spectrum Mill v4.01 (Agilent Technologies). MS/MS spectra with a sequence tag length of 1 or less were considered to be poor spectra and were discarded. The remaining MS/MS spectra were searched against the *Arabidopsis* TAIR10 proteome. The enzyme parameter was limited to tryptic peptides with a maximum mis-cleavage of 2. Carbamidomethylation was set as a fixed modification while Ox-Met, and phosphorylation on Serine, Threonine, or Tyrosine were defined as variable modifications. A maximum of 6 phosphorylation events per peptide was used. A 1:1 concatenated forward-reverse database was constructed to calculate the false discovery rate (FDR). The tryptic peptides in the reverse database were compared to the forward database, and were shuffled if they matched to any tryptic peptides from the forward database. Cutoff scores were dynamically assigned to each dataset to obtain a peptide false discovery rate (FDR) of 0.1%. Phosphorylation sites were localized to a particular amino acid within a phosphopeptide using the variable modification localization (VML) score in Agilent's Spectrum Mill software (Chalkley and Clauser, 2012).

QUANTIFICATION AND STATISTICAL ANALYSIS

RNA-seq Data Processing and Statistics

Raw reads were subject to quality control and trimming and aligned to the *Arabidopsis* TAIR10 reference genome using GSNAP (Wu and Nacu, 2010). Uniquely aligned reads were used to obtain read counts per gene. Only genes with an average read count greater than 1 across all samples were used for differential expression analysis. Normalization was conducted automatically by DESeq2, which corrects for biases introduced by differences in the total number of uniquely mapped reads between samples. Normalized read counts were used to calculate fold changes and test for differential expression. The R package DEseq2

(<https://bioconductor.org/packages/release/bioc/html/DESeq2.html>) was used to test the null hypothesis that expression of a given gene is not different between two genotypes or conditions being compared. This null hypothesis was tested using a model with a negative binomial distribution. P-values of all statistical tests were converted to adjusted p-values (q-values) (Benjamini and Hochberg, 1995). A false discovery rate of 10% (q-value) was used to account for multiple testing. Comparisons of gene lists were performed using Venny (<http://bioinfogp.cnb.csic.es/tools/venny/index.html>) and overrepresentation in overlapping gene lists tested using the Genesect tool in VirtualPlant (Katari et al., 2010). Reported overlaps were statistically significant at a $p < 0.05$ level. Clustering was performed using the ‘aheatmap’ function of the NMF package in R (<https://cran.r-project.org/web/packages/NMF/index.html>). Log2 reads per million mapped reads (RPM) values were used for clustering analysis and values were normalized for each gene by centering and scaling each row of the heatmap. GO analysis was performed using BINGO (Maere et al., 2005).

DATA AND SOFTWARE AVAILABILITY

RNA-seq data have been deposited into the Gene Expression Omnibus (GEO: GSE93420). Proteomics data relating to DSK2 phosphorylation by BIN2 have been deposited in the MassIVE repository (MassIVE: MSV000079641).

Developmental Cell, Volume 41

Supplemental Information

Selective Autophagy of BES1 Mediated by DSK2

Balances Plant Growth and Survival

Trevor M. Nolan, Benjamin Brennan, Mengran Yang, Jiani Chen, Mingcai Zhang, Zhaohu Li, Xuelu Wang, Diane C. Bassham, Justin Walley, and Yanhai Yin

Supplemental Inventory

Figure S1: BES1 and DSK2 interaction experiments. Related to Figure 1.

Figure S2: Confocal microscopy of BES1 and ATG8 in *Arabidopsis* protoplasts. Related to Figure 2.

Figure S3: BRZ response of *atg7-2* and *DSK2 RNAi* under non-stressed conditions. Related to Figure 3.

Figure S4: Interaction and phosphorylation of DSK2 by BIN2. Related to Figure 4.

Figure S5: BES1 transcript levels during stress treatments. Related to Figure 5.

Figure S6: Phenotypic and transcriptome changes during drought or dehydration stress. Related to Figure 5.

Figure S7: Effect of BIN2 and BES1 on drought stress phenotypes. Related to Figure 5.

Figure S8: Phenotypic and transcriptome changes during starvation stress. Related to Figure 6.

Figure S9: Effect of *SINAT RNAi* on BES1 accumulation and ubiquitination in during starvation. Related to Figure 7.

Table S1: DSK2 phosphorylation sites identified by mass spectrometry following *in vitro* phosphorylation with BIN2. Related to Figure 4.

Table S2: DSK2 mass spectrometry Spectrum Mill output. Related to Figure 4.

Table S3: Differentially expressed gene lists from RNA-seq experiments. Related to Figures 5 and 6.

Table S4: Summary of DSK2A variants used in this study. Related to Star Methods.

Table S5: Oligonucleotides used in this study. Related to Star Methods.

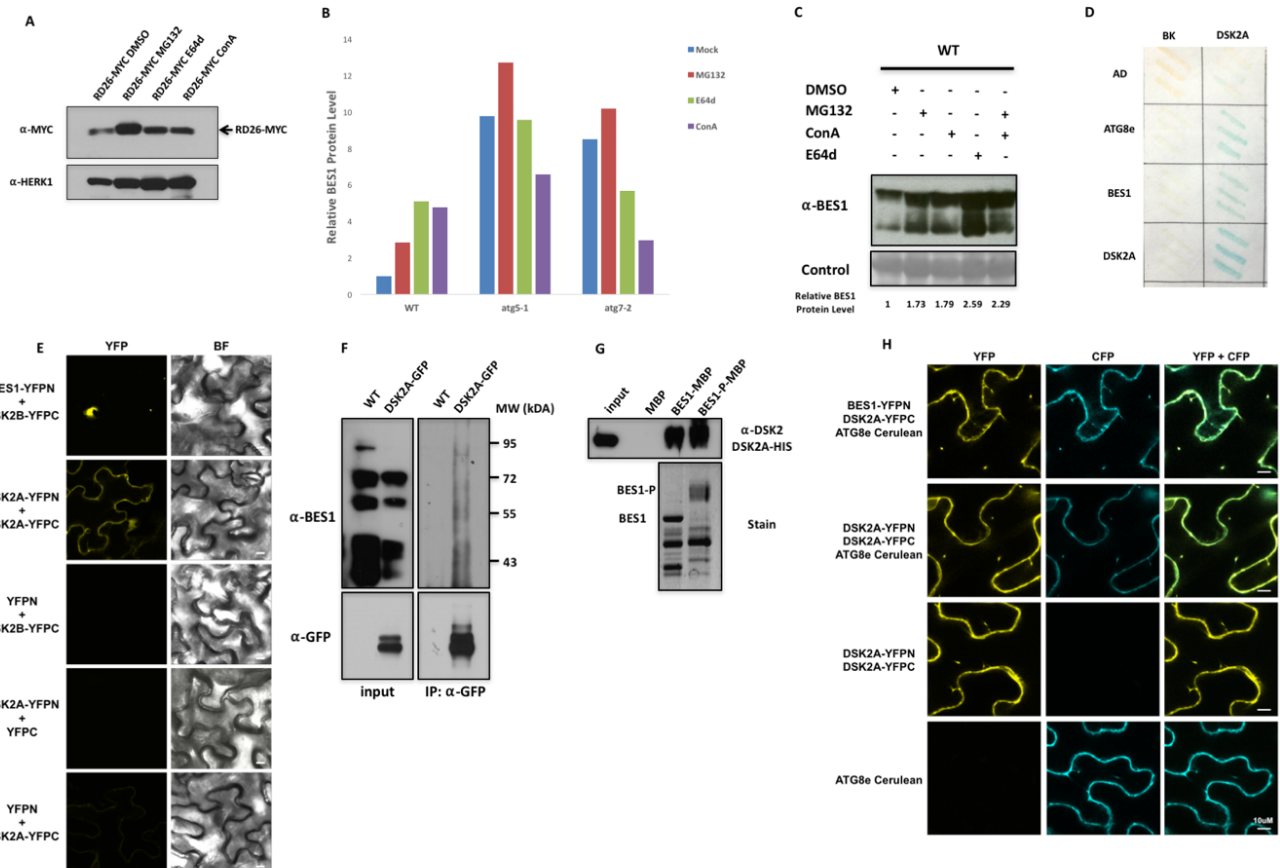


Figure S1: BES1 and DSK2 interaction experiments. Related to Figure 1.

(A) Control for proteasome and autophagy inhibitor treatments in Figure 1A and B. MYC-tagged RD26 transgenic plants were treated for 6 hours in 1/2 MS liquid with DMSO, 50μM MG132, 20μM E64d or 1μM ConA. RD26-MYC protein was detected by western blotting with anti-MYC antibodies. HERK1 served as a loading control.

(B) Quantification of BES1 protein levels following inhibitor treatments from Figure 1B.

(C) BES1 accumulation after combined proteasome and autophagy inhibitor treatment. Plants were treated for 6 hours in 1/2 MS liquid with DMSO, 50μM MG132, 20μM E64d or 1μM ConA, or both 50μM MG132 and 1μM ConA.

(D) LacZ assays showing yeast-two hybrid interactions of DSK2A with BES1 or ATG8e and self-association of DSK2A.

(E) BiFC assays in *N. benthamiana* showing interactions of BES1 with DSK2B (top panel) or DSK2A self-association (second panel). Negative controls are shown in bottom panels.

(F) Co-Immunoprecipitation showing interaction of DSK2-GFP with high-molecular weight forms of BES1. WT or 35S:DSK2-GFP plants were treated with 1μM ConA and 2μM Brassinazole (BRZ) for 16 hours. Co-IP was performed with anti-GFP antibodies and BES1 detected with anti-BES1 antibody.

(G) Interaction of DSK2-HIS with BES1-MBP and phosphorylated BES1-MBP. Equal amounts of BES1-MBP protein were incubated with BIN2-GST in the absence (unphosphorylated BES1) or presence of ATP (phosphorylated BES1). Pulldown reactions were then carried out by incubating DSK2A-HIS with MBP, BES1-MBP or phosphorylated BES1-MBP. MBP proteins were bound with amylose resin and interacting DSK2-HIS detected with anti-DSK2 antibodies. SYBR Ruby staining was used to verify the phosphorylation status of BES1 (lower panel).

(H) BiFC colocalization assays in *N. benthamiana* showing colocalization of BES1-DSK2A or DSK2A-DSK2A complexes (YFP channel) with autophagy marker Cerulean-ATG8e (CFP channel). Top panel showing DSK2A-BES1 colocalization with Cerulean-ATG8 is repeated from Figure 1H to show specificity of channels. Bottom panels indicate expression of YFP signals only (DSK2A-YFPN with DSK2A-YFPC) or CFP signals only (Cerulean-ATG8e). Scale bars for BiFC experiments indicate 10 μ m.

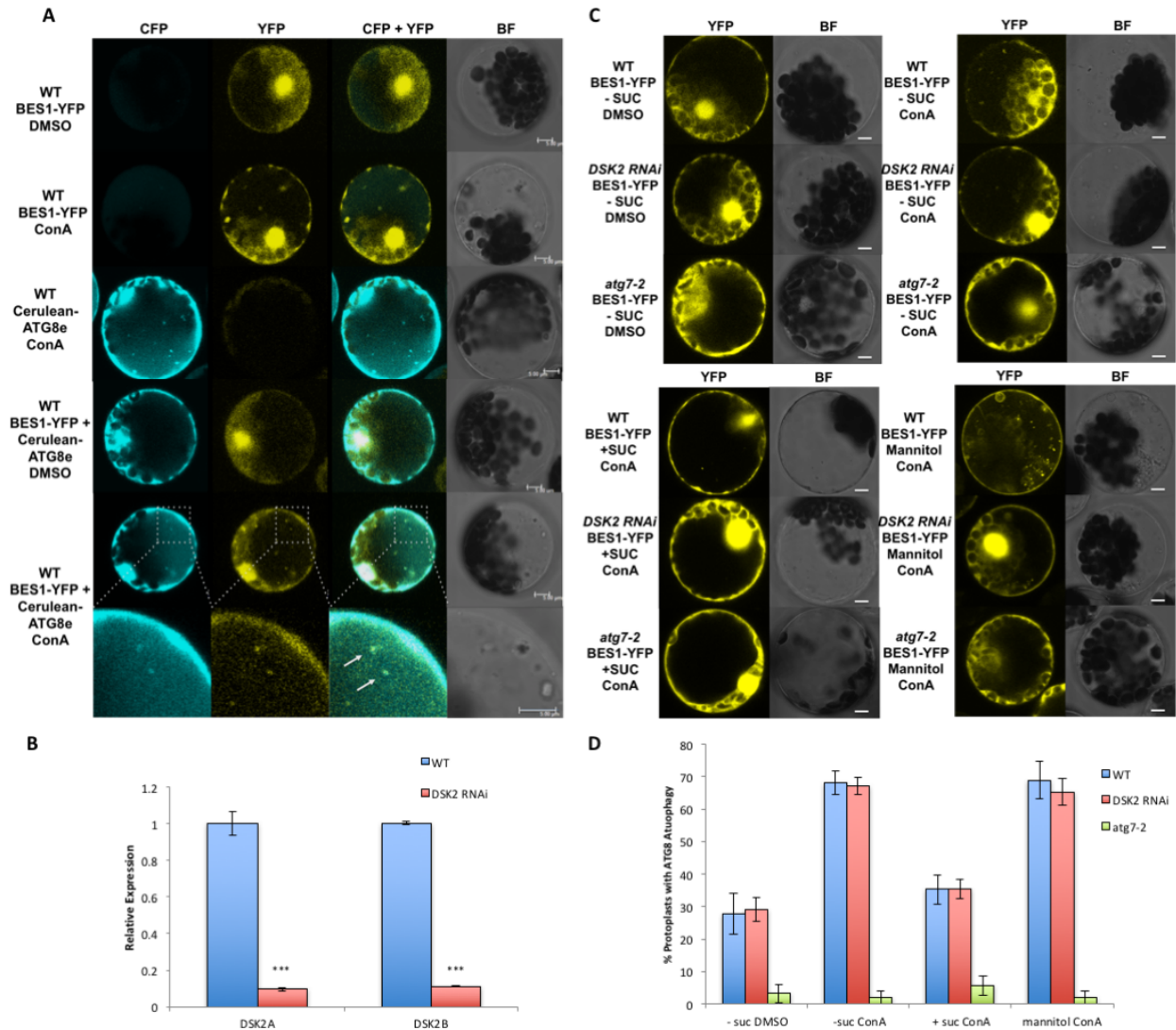


Figure S2: Confocal microscopy of BES1 and ATG8 in *Arabidopsis* protoplasts. Related to Figure 2.

(A) Protoplasts treated with starvation (-Suc) conditions were incubated with control solvent (DMSO) or 1 μ M ConA for 12 hours and imaged by confocal microscopy. CFP, YFP or merged (CFP + YFP) fluorescence channels are shown along with bright field images (BF). Single transformations of BES1-YFP (top two panels) or Cerulean-ATG8e (third panel) indicate that CFP and YFP channels are specific. Arrows denote ATG8-labeled autophagosomes that colocalize with BES1 (bottom panel). Bright field images are shown (BF).

(B) mRNA expression levels of DSK2A and DSK2B in WT or *DSK2 RNAi* plants from whole transcriptome RNA-seq. Error bars represent SEM (***, p< 0.001, t test).

(C) Representative images of protoplasts expressing BES1-YFP used for quantification of protoplasts containing BES1 autophagy in Figure 2D. WT expressing BES1-YFP under -Suc DMSO conditions was a shared control and is also presented in Figure 1D.

(D) Quantification of protoplasts containing ATG8 autophagy using Cerulean-ATG8e marker. ATG8 autophagy was defined by the presence ≥ 3 Cerulean-ATG8 labeled autophagosomes per protoplast.

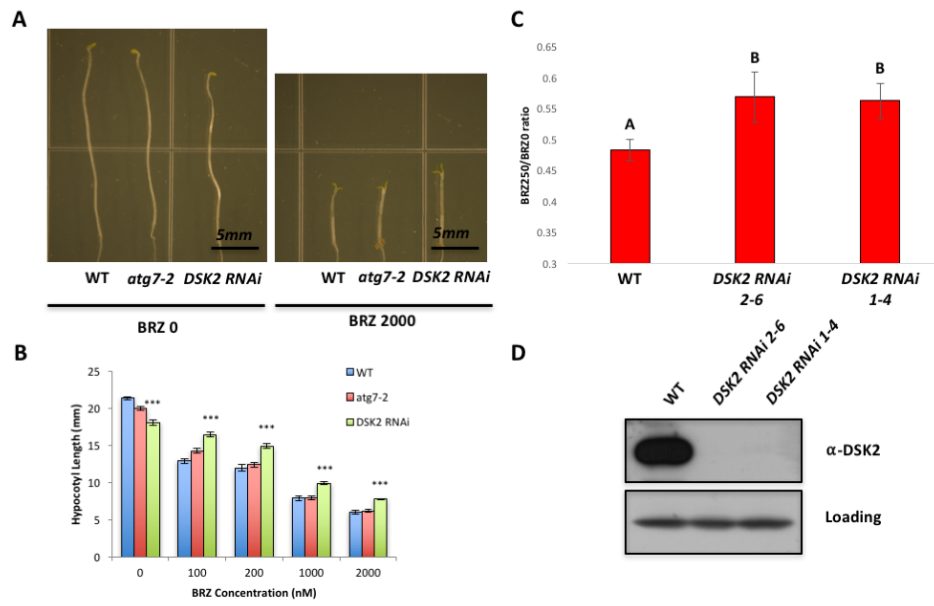


Figure S3: BRZ response of *atg7-2* and *DSK2 RNAi* under non-stressed conditions.
Related to Figure 3.

(A) Plant phenotypes in BRZ response assay. Plants were grown on control or BRZ containing medium in darkness for 7 days followed by imaging and hypocotyl length measurements.
 (B) Quantification of hypocotyl length from BRZ response assays. Data represent mean \pm SEM from at least 10 seedlings. (***, p < 0.001, t test.).
 (C) BRZ response under non-stress conditions with an additional independent *DSK2 RNAi* line. *DSK2 RNAi* 2-6 is otherwise referred to as *DSK2 RNAi* throughout this study.
 (D) *DSK2* protein levels in *DSK2 RNAi* lines detected using anti-*DSK2* antibodies. IWS1 was used as a loading control.

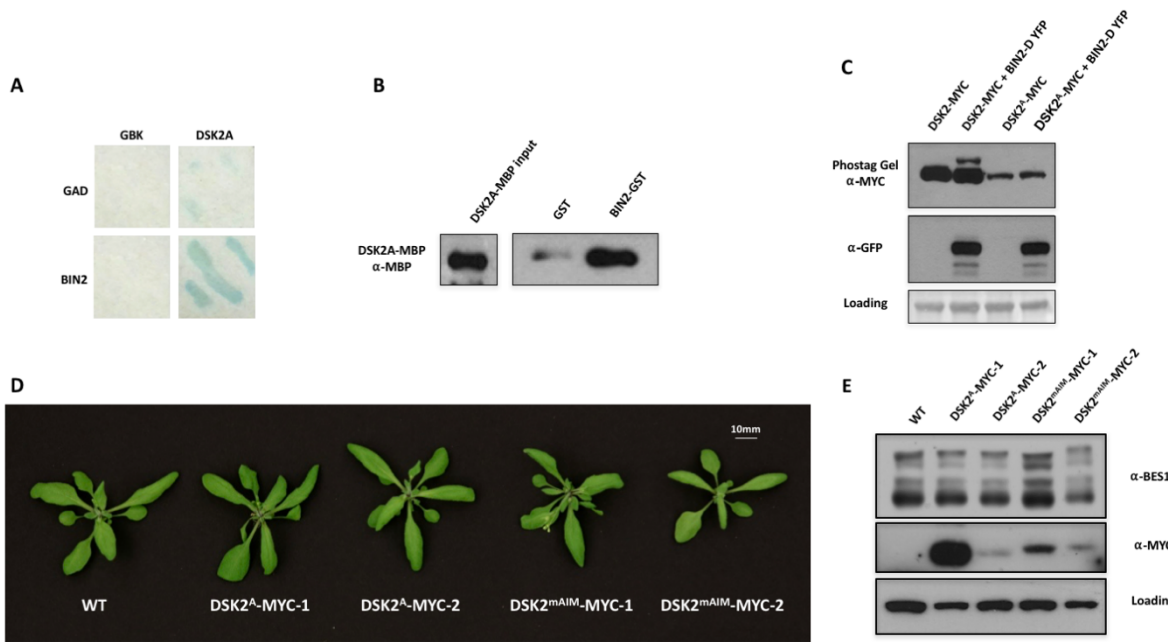


Figure S4: Interaction and phosphorylation of DSK2 by BIN2. Related to Figure 4.

(A) Interaction of DSK2A with BIN2 in yeast-two hybrid LacZ assays.

(B) GST pulldown showing interaction of DSK2A-MBP with BIN2-GST. DSK2A-MBP was detected using anti-MBP antibody.

(C) Phosphorylation of DSK2 upon coexpression with BIN2 in *N. benthamiana*. DSK2-MYC or DSK2^A-MYC (with predicted BIN2 phosphorylation sites mutated to Ala) was co-expressed with empty vector control or with BIN2-D YFP. After 48 hours, protein was extracted and analyzed by SDS-PAGE using anti-GFP antibodies to detect BIN2-YFP or by Phostag SDS-PAGE with anti-MYC antibodies to detect DSK2-MYC fusion proteins.

(D) Phenotype T2 transgenic lines overexpressing DSK2 mutant forms shown in Figure 1D.

(E) BES1 protein levels in DSK2-MYC lines. Protein extracts from indicated lines were analyzed by western blotting. DSK2-MYC mutant forms were detected with anti-MYC antibodies, while BES1 was detected with anti-BES1. A non-specific band from anti-MYC was used as a loading control.

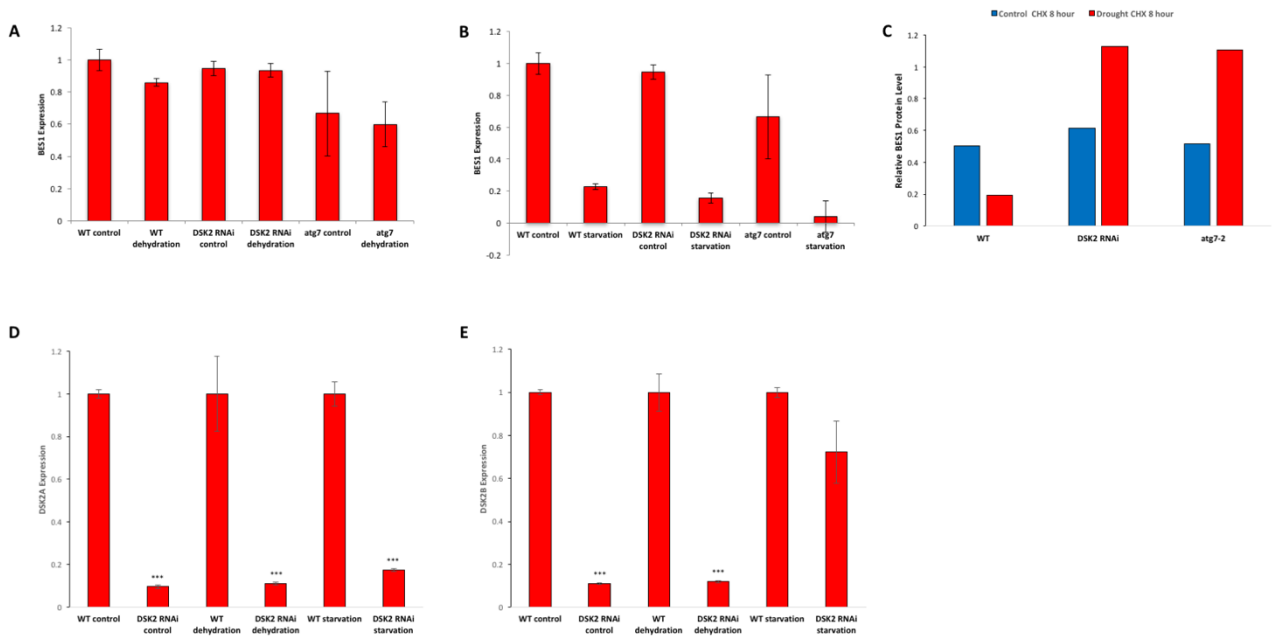


Figure S5: BES1 transcript levels during stress treatments. Related to Figure 5.

- (A) BES1 transcript levels during dehydration treatments as monitored by whole transcriptome RNA-seq.
- (B) BES1 transcript during starvation treatments as monitored by whole transcriptome RNA-seq.
- (C) Quantification of BES1 protein levels from cycloheximide (CHX) treatments shown in Figure 5D. Relative BES1 level is defined as BES1 after 8hr CHX treatment/BES1 at 0 hr.
- (D) DSK2A transcript levels during control and indicated stress treatments as monitored by whole transcriptome RNA-seq.
- (E) DSK2B transcript levels during control and indicated stress treatments as monitored by whole transcriptome RNA-seq. All error bars in this figure indicate SEM (***, p<0.001, t test).

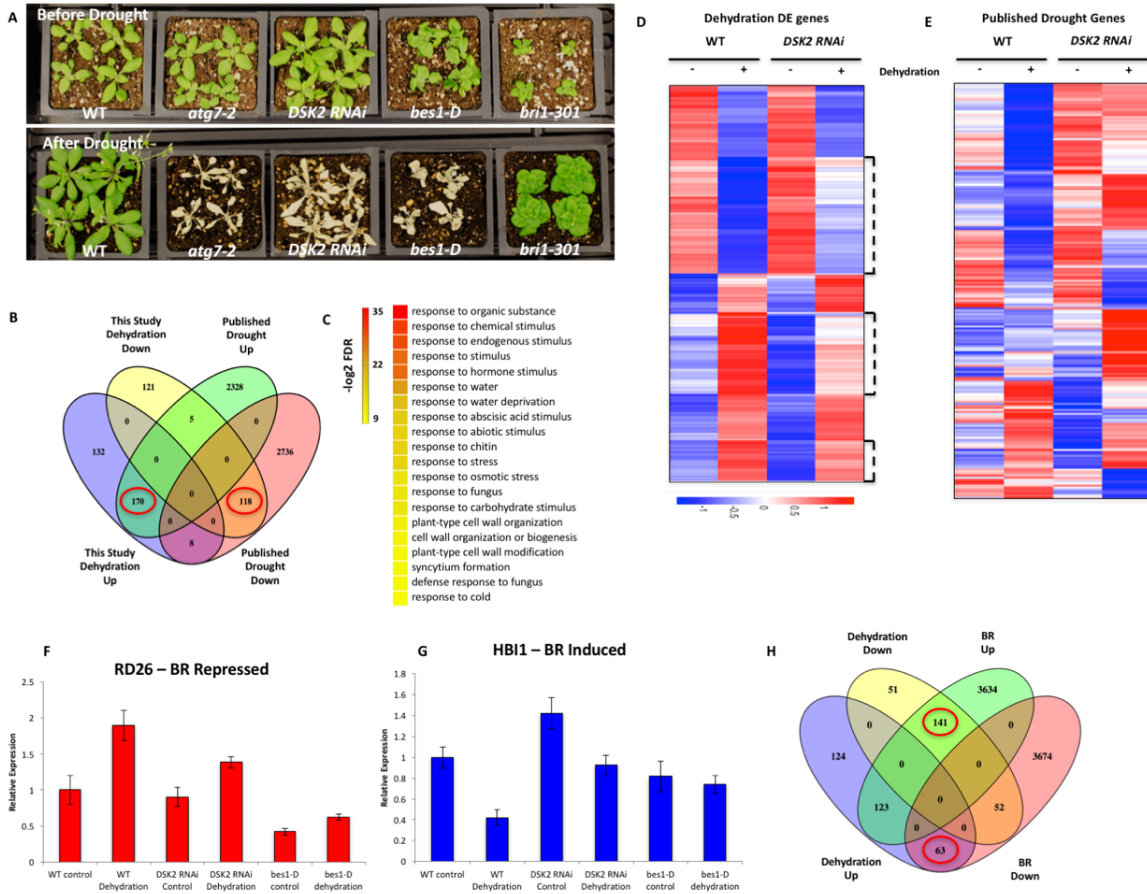


Figure S6: Phenotypic and transcriptome changes during drought or dehydration stress. Related to Figure 5.

(A) Additional drought phenotype images from drought assay described in Figure 6A. Plants were imaged before significant drought stress was imposed (Before Drought) followed by drought treatment and rewetting. Plants were imaged again 7 days subsequent to rewetting (After Rewatering).

(B) Comparison of RNA-seq dehydration regulated genes to previously published drought regulated genes.

(C) Top 20 significantly enriched GO terms in Dehydration regulated genes as ranked by false discovery rate (FDR).

(D) Clustering analysis of 554 genes DE during WT dehydration treatments. Brackets indicate clusters of genes with altered expression patterns in *DSK2 RNAi* plants.

(E) Clustering of 5,365 genes previously implicated in drought response using dehydration RNA-seq data from this study. Color legend indicates normalized gene expression values.

(F) Expression levels of RD26 from RNA-seq experiments. RD26 is a known dehydration induced gene that is down regulated in *DSK2 RNAi* and *bes1-D* during compared to WT dehydration. Error bars indicate SEM.

(G) Expression levels of HBI1 from RNA-seq experiments. HBI1 is a positive regulator in growth that is downregulated during dehydration in WT, but not in *DSK2 RNAi* and *bes1-D*. Error bars indicate SEM.

(H) Overlap of dehydration DE genes with Brassinosteroid (BR) regulated genes showing enrichment of dehydration down regulated genes that were upregulated by BRs (57.8%, 141/244) and dehydration upregulated genes that were downregulated by BRs (20.3%, 63/310).

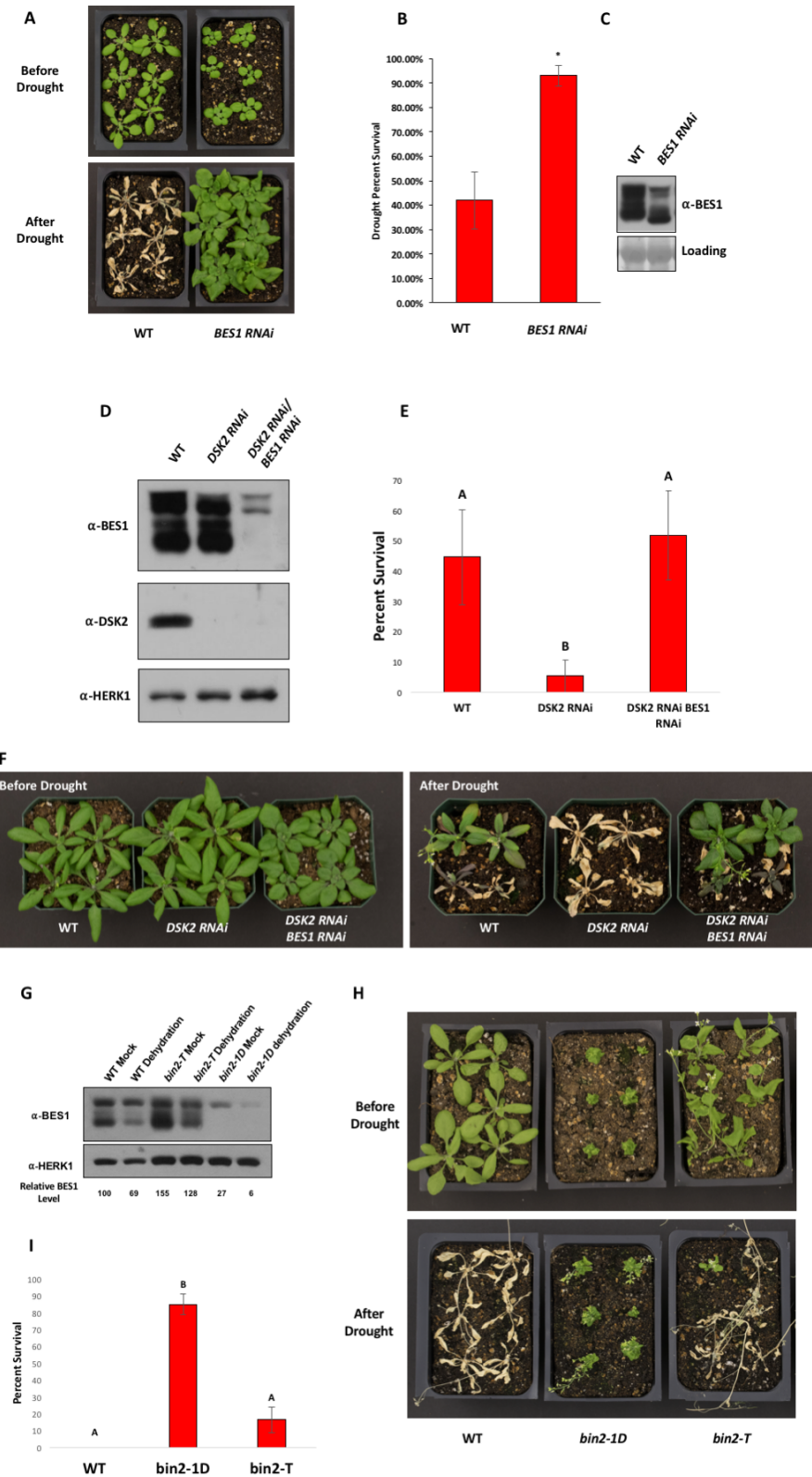


Figure S7: Effect of BIN2 and BES1 on drought stress phenotypes. Related to Figure 5.

- (A) Phenotype of *BES1 RNAi* during drought stress. Plants were imaged before significant drought stress was imposed (Before Drought) followed by drought treatment and rewetting. Plants were imaged again 7 days subsequent to rewetting (After Rewetting).
- (B) Quantification of percent survival following drought recovery from (A). Plants producing new leaves after the 7-day recovery period were scored as survivors. Data represent mean survival of 3 biological replicates of at least 12 plants ± SEM, (*p < 0.05, t test).
- (C) BES1 protein levels are reduced in *BES1 RNAi* plants as monitored by western blotting with anti-BES1 antibody.
- (D) Both BES1 and DSK2 protein levels are reduced in *DSK2 RNAi BES1 RNAi* plants.
- (E) Quantification of percent survival following drought recovery for *DSK2 RNAi* and *DSK2 RNAi BES1 RNAi*. Plants producing new leaves after the 7-day recovery period were scored as survivors. Data represent mean survival of 3 biological replicates of at least 8 plants ± SEM. Different letters indicate statistically significant differences p<0.05, t test.
- (F) Drought stress phenotypes of *DSK2 RNAi* and *DSK2 RNAi BES1 RNAi* double mutants. Plants were imaged before significant drought stress was imposed (Before Drought) followed by drought treatment and rewetting. Plants were imaged again 7 days subsequent to rewetting (After Rewetting).
- (G) BES1 protein levels in *bin2* gain-of-function (*bin2-1D*) and loss-of-function (*bin2-T*) mutants during dehydration treatments. Plants were subjected to control or 4-hour dehydration conditions and BES1 levels analyzed by western blotting. HERK1 was used as a loading control.
- (H) Drought stress phenotypes of *bin2* mutants. Plants were imaged before significant drought stress was imposed (Before Drought) followed by drought treatment and rewetting. Plants were imaged again 7 days subsequent to rewetting (After Rewetting).
- (I) Quantification of percent survival following drought recovery for *bin2* mutants. Plants producing new leaves after the 7-day recovery period were scored as survivors. Data represent mean survival of 3 biological replicates of at least 10 plants ± SEM. Different letters indicate statistically significant differences p<0.05, t test.

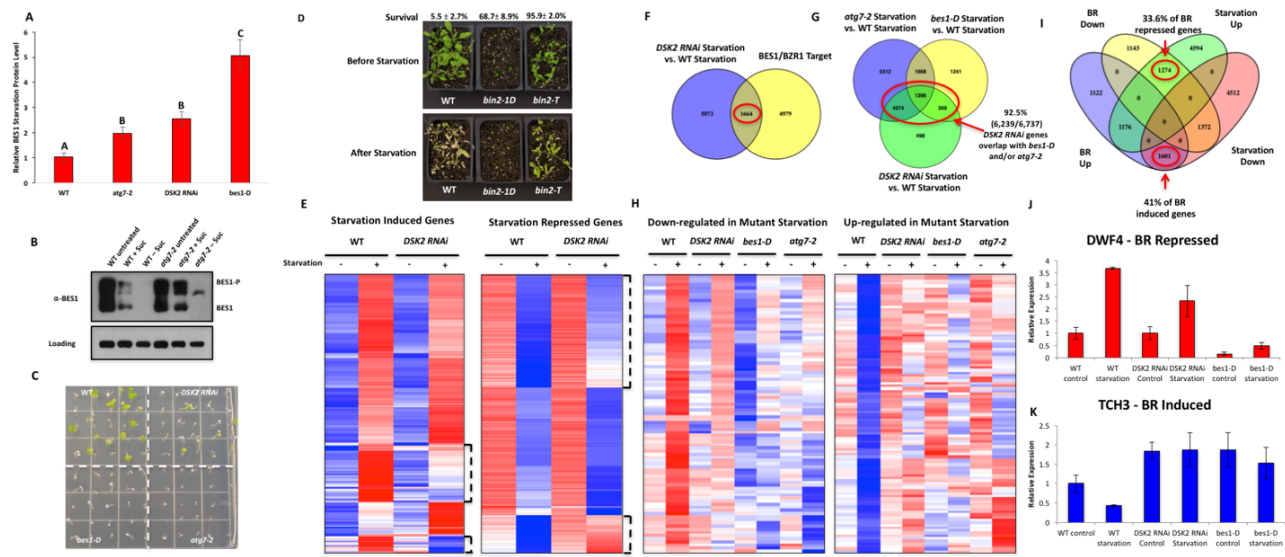


Figure S8: Phenotypic and transcriptome changes during starvation stress. Related to Figure 6.

(A) Quantification of BES1 protein levels during starvation as shown in Figure 6C. Data represent mean BES1 protein level \pm SEM from 3 biological replicates (for WT, *atg7-2* and *DSK2 RNAi*) or 2 biological replicates (*bes1-D*). Different letters indicate statistically significant differences $p<0.05$, t test.

(B) BES1 protein levels are regulated by energy availability in dark conditions. Protein samples were collected from 7 day-old WT or *atg7-2* seedlings that were untreated or transferred to plates with (+ Suc) or without sucrose (-Suc) and incubated in darkness for three days. Western blotting was performed with anti-BES1 antibodies or anti-HERK1 (loading control).

(C) Representative image showing fixed-carbon starvation survival phenotypes after 10 days darkness as presented in Figure 7B.

(D) Phenotypes of *bin2* mutants after starvation stress. Representative images of plant survival following 9 day fixed-carbon starvation treatment. Percentage survival is indicated from 3 biological repeats of at least 12 plants \pm SEM. Differences between WT and mutants are statistically significant $p<0.05$ (t test).

(E) Clustering of 7044 starvation upregulated genes (left panel) or 7485 starvation downregulated genes (right panel). Brackets indicate clusters of genes with altered expression patterns in *DSK2 RNAi* plants.

(F) Comparison of *DSK2 RNAi* starvation DE genes with BES1/BZR1 target genes.

(G) Overlap of genes DE in *atg7-2*, *bes1-D*, or *DSK2 RNAi* starvation compared to WT starvation.

(H) Clustering of 89 genes upregulated during starvation but downregulated in *DSK2 RNAi*, *bes1-D*, and *atg7-2* starvation (left panel) or 106 genes downregulated during starvation but upregulated in *DSK2 RNAi*, *bes1-D*, and *atg7-2* starvation (right panel).

(I) Comparison of starvation DE genes with Brassinosteroid (BR) regulated genes.

(J) Expression levels of DWF4 from RNA-seq experiments. Error bars indicate SEM.

(K) Expression levels of TCH3 from RNA-seq experiments. Error bars indicate SEM.

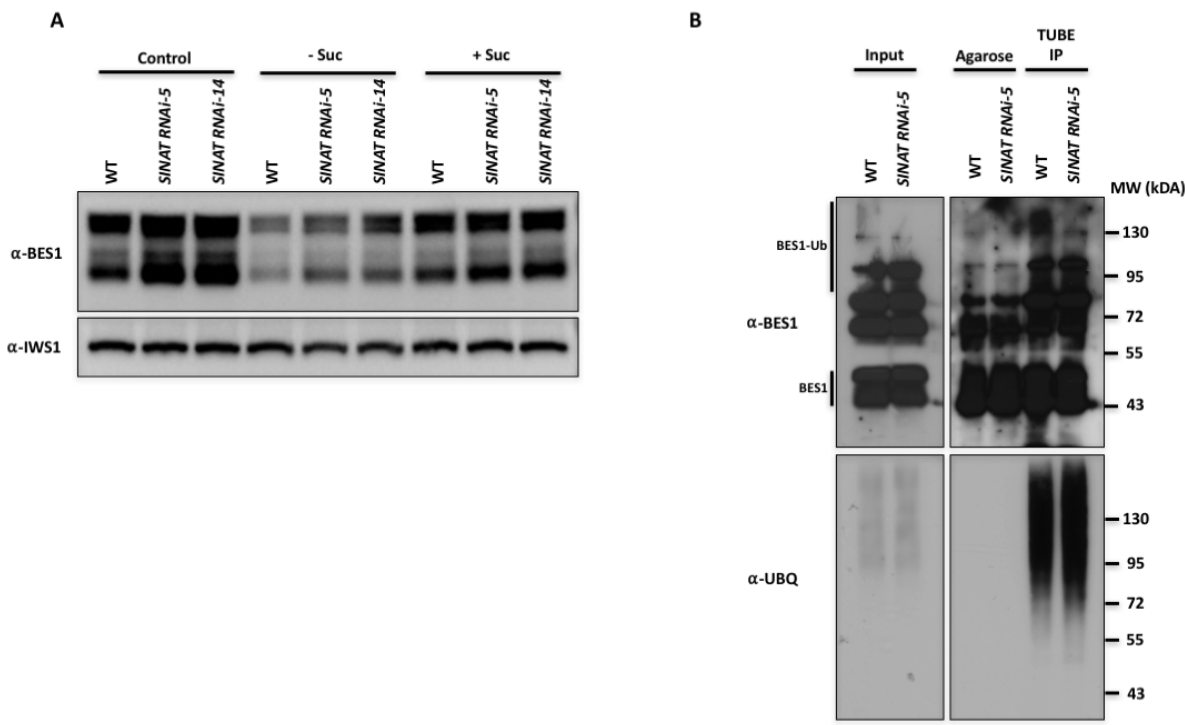


Figure S9: Effect of *SINAT RNAi* on BES1 accumulation and ubiquitination during starvation. Related to Figure 7.

(A) Western blot analysis of BES1 protein levels from 10-day seedlings in WT and two independent *SINAT RNAi* lines. Plants were harvested directly after 10 days of growth (Control) or transferred to plates without sucrose (-Suc) or with sucrose (+Suc) and incubated for 3 days in darkness. IWS1 served as a loading control.

(B) Ubiquitinated BES1 is reduced in *SINAT RNAi* during starvation. Tandem Ubiquitin Binding Entities (TUBE) ubiquitination assays were performed with 10-day old WT or *SINAT RNAi* seedlings treated with – sucrose and 20 μ M E64d in darkness for 24 hours. Input, control (Agarose) and ubiquitin enriched (TUBE IP) samples were analyzed by western blotting with BES1 and Ubiquitin (UBQ) antibodies.

Table S1: DSK2 phosphorylation sites identified by mass spectrometry following *in vitro* phosphorylation with BIN2. Related to Figure 4.

DSK2 Phosphorylation Site(s)	Number of Phosphorylated Residues	Peptide Sequence
S7	1	(2)GGEADsRQPLTAEGVAVAVNVR(23)
T12	1	(9)QPLtAEGVAVAVNVR(23)
S7 or T12 or T28 or S31 or T33 or T34 or S35 or S38 or T39	4	(5)ADSRQPLTAEGVAVAVNV RCSNGTKFSVTTSLDSTVE(41)
S31 or T33 or T34 or S35 or S38 or T39 or S42	1	(30)FSVTTSLDSTVESFK(44)
T172	1	(168)EMMNTPAIQNLMMNNPE FMR(186)
S213	1	(197)ELVDRNPELGHVLNDPSI LR(216)
S213 or T218	1	(205)LGHVLNDPSILRQTLE(220)
S240	1	(238)AMSNIESMPEGFNMLR (253)
S244	1	(238)AMSNIESMPEGFNMLR (253)
S425 or S426	1	(414)MMQNPDFLRQFSSPE(428)
S425 or S426 or S435 or S439 or S442	1	(423)QFSSPEMMQQMMSLQQSLFSQNR(445)
T447 or T453 or T455 or T459 or T461 or S476 or S483 or T485	3	(446)NTAGQDPQTGTGAATGT ANNGGLDLLMNMFGSLGAG GLSGTNQPNVPPEER(495)
T521	1	(514)NIRALLatNGNVNAAVE(530)

Phosphorylation sites flanking DSK2 AIM domains are bold. When phosphorylation sites could not be localized due to peptide fragmentation patterns, all possible residues are listed. Number of phosphorylated residues indicates sites detected within a single peptide. No phosphorylation was detected in mock DSK2 phosphorylation reactions lacking BIN2. For complete output of DSK2 mass spectrometry data see Table S2.

Table S4: Summary of DSK2A variants used in this study. Related to Star Methods.

Construct	Phosphorylation site mutations	AIM mutations	Region
DSK2 ^D	S31D T34D S35D S38D T39D S42D S114D S118D S240D S244D T292D S296D S299D S303D T324D T328D T362D S366D S435D S439D T455D T459D	None	Full Length 1-538
DSK2 ^A	S31A T34A S35A S38A T39A S42A S114A S118A S240A S244A T292A S296A S299A S303A T324A T328A T362A S366A S435A S439A T455A T459A	None	Full Length 1-538
DSK2 ^A mAIM	S31A T34A S35A S38A T39A S42A S114A S118A S240A S244A T292A S296A S299A S303A T324A T328A T362A S366A S435A S439A T455A T459A	F43A L46A F249A L252A Y256A V259A	Full Length 1-538
DSK2 mAIM	None	F43A L46A F249A L252A Y256A V259A	Full Length 1-538
DSK2 ^{D12}	S31D T34D S35D S38D T39D S42D S114D S118D S240D S244D	None	Full Length 1-538
DSK2 ^{A12}	S31A T34A S35A S38A T39A S42A S114A S118A S240A S244A	None	Full Length 1-538
DSK2 C1	None	None	90-538
DSK2 C2	None	None	403-538
DSK2AΔUBA	None	None	1-497

Table S5: Oligonucleotides used in this study. Related to Star Methods.

Oligo Name	Sequence
DSK2AF	CACCGAATTCGGTACCATGGTGGTGAAGCAGATTGAGG
DSK2AR	CACCGTCGACCTGCCAATACTCCCCAAGAGTCGT
DSK2AGSTF	CACGAATTCATGGTGGTGAAGCAGATTGAGG
DSK2AGSTR	CACGTCGACTTACTGCCAATACTCCCCAAGA
DSK2AC1F	CACCGAATTCTTGTGCCTCTCCTCTGCTCC
DSK2AC2F	CACCGAATTCAAGCATGCTAGATATGAATCCTCAGT
DSK2AUBAdel	CACCGTCGACCGCAAATCGCTTCAGGAGGAACA
DSK2BGSTF	CACCGAATTCATGGTGGAGAGGGAGATTCAAGTCA
DSK2GSTR	CACCGTCGACCTACTGTCCGATACTCCCCAAGA
ATG8aF	CACCGGATCCATGATCTTGCTTGCTGAAATTGCA
ATG8aR	CACCGTCGACTCAAGCAACGGTAAGAGATCCAAAAGT
ATG8eGSTF	CACCGGATCCATGAATAAAGGAAGCATTTAAGATGGACA
ATG8eGSTR	CACCGCGGCCGCTTAGATTGAAGAACCGAATGT
ATG8fF	CACCGAATTCATGGCAAAAGCTCGTTCAAGCAAGA
ATG8fR	CACCGTCGACTTATGGAGATCCAATCCAATGTGT
ATG8iF	CACCGAATTCAAGGTTTCTCACTGCTA
ATG8iR	CACCGTCGACTCAACCAAAGGTTTCTCACTGCTA
BIN2F	CACCGGATCCACCATGGCTGATGATAAGGAGATGCCTGC
BIN2R	CACCGTCGACTTAAGTCCAGATTGATTCAAGAAGCT